Gondwana Research 60 (2018) 129–152

Contents lists available at ScienceDirect

Gondwana Research

journal homepage: www.elsevier.com/locate/gr

Composition and source of fluids in high-temperature graphite-bearing granitoids associated with granulites: Examples from the Southern Marginal Zone, Limpopo Complex, South Africa

Oleg G. Safonov [a,b,c,*], Vadim N. Reutsky [d], Dmitriy A. Varlamov [a], Vasily O. Yapaskurt [b], Maria A. Golunova [a], Vasily D. Shcherbakov [b], Dirk D. van Reenen [c], Andre C. Smit [c], Valentina G. Butvina [a]

[a] Institute of Experimental Mineralogy, Russian Academy of Sciences, Academician Ossipyan str., 4, Chernogolovka, Moscow 142432, Russia
[b] Department of Petrology, Moscow State University, Moscow, Russia
[c] Department of Geology, University of Johannesburg, Johannesburg, South Africa
[d] Institute of Geology and Mineralogy, Siberian Branch, Russian Academy of Sciences, Novosibirsk, Russia

ARTICLE INFO

Article history:
Received 26 June 2017
Received in revised form 13 March 2018
Accepted 6 April 2018
Available online 05 May 2018

Handling Editor: T. Tsunogae

Keywords:
Orthopyroxene-bearing metapelite
Trondhjemite
Tonalite
Granite
Phase equilibria modeling
Graphite
Carbon isotopes
Fluids
Limpopo Complex

ABSTRACT

P-T conditions, fluid regime and carbon isotope composition of graphite and fluid inclusions from garnet-sillimanite-bearing leucocratic tonalites, trondhjemites and granites associated with orthopyroxene-bearing granulite metapelites in the Southern Marginal Zone (SMZ) of the Limpopo Complex, South Africa, are presented in the paper. Re-integrated compositions of perthitic alkali feldspars and antiperthitic plagioclase, as well as P-T and T-X_{CO2} phase equilibria modeling using PERPLE_X software indicate that the granitoids began to crystallize at temperatures of 900–940 °C and pressures of 7–9 kbar, and were equilibrated with a fluid phase with $X_{CO2} > 0.5$–0.6 as is recorded in dense fluid inclusions in quartz. A small fraction of a saline fluid accumulated during cooling only. Average $\delta^{13}C_{PDB}$ values for graphite (−6.52 to −8.65‰) and fluid inclusions (−2.50 to −5.58‰) from the granitoids differ substantially from the values, which have been obtained in previous studies for graphite from the surrounding SMZ metapelites. Isotope data thus indicate that fluids associated with the granitoid magmas of the SMZ originated from a source unrelated to the host metapelites. In terms of the "heavy" isotope signatures of carbon, the granitoids might carry fluids, which have been produced during devolatilization of mafic rocks (amphibolites) interlayered with hydrothermal carbonate veins in the adjacent granite-greenstone successions of the Kaapvaal craton that have been buried underneath the SMZ granulites during their exhumation. The cratonic rock could serve as a source for the trondhjemite magmas intruding the SMZ granulites. In this scenario, the studied granitoids crystallized from these magmas variously contaminated by metapelitic material. Graphite precipitated via reduction of CO_2-rich fluid as the result of dissolution of pyrrhotite-rich metapelites in the magmas.

1. Introduction

Carbon dioxide is a principal component of fluids acting during upper-amphibolite and granulite-facies metamorphism in the middle to lower crust. Widespread findings of dense CO_2 inclusions in minerals of high-grade rocks inspired in the 1980s (e.g. Newton et al., 1980) the development of the "carbonic model" for granulite metamorphism. This model considers the leading role of pervasive flushing of external (mostly, upper mantle-related) CO_2-rich fluids in the formation of granulite assemblages (e.g. Santosh and Omori, 2008). However, many arguments were put forward against the "carbonic model" (e.g. Lamb and Valley, 1985; Stevens and Clemens, 1993), which were mainly based on the identification of localized action of CO_2 recorded, in particular, in carbon isotopic gradients in granulites (Lamb and Valley, 1985; Vennemann and Smith, 1992; Stevens, 1997). These arguments were in line with experimental data on the limited migration scale of CO_2 through crystalline rocks (Watson and Brenan, 1987). They provided a basis for alternative models to explain abundant CO_2 recorded in granulites: post-peak entrapment of carbonic inclusion (e.g. Lamb et al., 1987), oxidation of graphite-bearing sediments by H_2O (Touret, 1971; Whitney, 1992; Giorgetti et al., 1996; Stevens, 1997), Fe^{3+} reduction in graphitic metapelites (Hollister, 1988; Cesare et al., 2005), sulfide-silicate-graphite reactions (e.g. Tracy and Robinson, 1988), modifications of CO_2-bearing fluid inclusions (e.g. Hollister, 1990), derivation from decarbonation of siliceous carbonate rocks (e.g. McLelland et al., 1988; Todd and Evans, 1993), immiscibility in H_2O-CO_2-salt fluids (e.g. Newton et al., 2014 and references therein).

* Corresponding author.
E-mail address: oleg@iem.ac.ru (O.G. Safonov).

https://doi.org/10.1016/j.gr.2018.04.009
1342-937X/

Most conflicting data on the role of CO_2 in granulites can be partially reconciled by assuming that CO_2 can be transported by magmas both produced during anatexis and injected from external sources. CO_2 has low solubility in silicic magmas at crustal pressures (<0.9 wt%; see Ni and Keppler, 2013 for compilation of experimental data). This fact is used by some authors (e.g. Stevens, 1997) as proof for insignificant participation of magmatic CO_2 during high-grade metamorphism. However, many researchers (e.g. Holloway, 1976; Frost and Frost, 1987; Frost et al., 1989; Lowenstern, 2001) consider that CO_2 could coexist as a free fluid phase with silicic magmas buffering water activity and assisting with the ascent of the magmas. Being transported by granitic magmas, poorly soluble CO_2 is able to interact with surrounding rocks (e.g. Farquhar and Chacko, 1991; Satish-Kumar and Santosh, 1998).

One of the principal indicators of fluid-rock interaction during granulite formation is graphite (e.g. Santosh and Omori, 2008; Huizenga, 2011; Huizenga and Touret, 2012; Luque et al., 2012). As a syngenetic mineral, graphite appears during graphitization of organic substances or through reduction of carbonates dispersed in a pre-metamorphic protolith (e.g. Wada et al., 1995). However, epigenetic graphite can also be precipitated from CO_2-bearing fluids generated during metamorphism, or can be released from magmas interacting with rocks during metamorphism being a function of pressure, temperature, rock-buffered low oxygen fugacity, CO_2 mole fraction in fluids, and the fluid/rock ratio (e.g. Glassley, 1982; Lamb and Valley, 1985; Huizenga, 2011; Huizenga and Touret, 2012). Therefore, the presence of graphite is used as evidence in support of the carbonic model (Farquhar and Chacko, 1991; Santosh and Wada, 1993; Radhika and Santosh, 1996; Satish-Kumar, 2005; Santosh and Omori, 2008; Satish-Kumar et al., 2011; Huizenga and Touret, 2012), while its absence is an argument against this model (Glassley, 1982; Lamb and Valley, 1985).

In this context, graphite behavior during crustal anataxis is of obvious interest. In many cases, primary graphite disappears during partial melting owing to oxidation by aqueous fluids (e.g. Touret, 1971; Whitney, 1992; Giorgetti et al., 1996; Stevens, 1997) or by Fe^{3+} released after biotite decomposition (Hollister, 1988; Cesare et al., 2005) producing CO_2. Nevertheless, graphite is recorded in granitoid leucosomes and dykes associated with granulites (Jackson et al., 1988; Farquhar and Chacko, 1991; Radhika and Santosh, 1996; Satish-Kumar and Santosh, 1998; Satish-Kumar et al., 2011; Rodas et al., 2000), and is preserved in peraluminous silicic plutonic bodies and lavas originated from crustal anataxis (Zeck, 1970; Duke and Rumble, 1986; Kanaris-Sotiriou, 1997). The above studies showed that during anataxis, graphite could be either inherited from the country rocks or precipitated via reduction of CO_2-bearing fluids released by magmas. Inferences on the carbon and graphite source during anatexis are predominantly based on isotopic characteristics of both graphite and fluid inclusions in segregations produced by this process (Jackson et al., 1988; Santosh et al., 1991; Farquhar and Chacko, 1991; Radhika and Santosh, 1996; Rodas et al., 2000; Satish-Kumar et al., 2011). The $\delta^{13}C_{PDB}$ values vary from <−20‰ for the inherited graphite (e.g. Rodas et al., 2000) up to −9 to −6‰ for epigenetic graphite (e.g. Farquhar and Chacko, 1991), although these two sources can be mixed too (e.g. Radhika and Santosh, 1996). Heavy values correspond to so-called "mantle signature" (e.g. Valley, 1986; Kyser, 1986; Javoy et al., 1986; Luque et al., 2012) suggesting a possible participation of the mantle source of carbon in fluids transported by granitic magmas. However, $\delta^{13}C_{PDB}$ values, which are close to the "mantle signatures", can be also attained as a result of the carbon isotope fractionation during graphite precipitation from CO_2-rich fluid on cooling (e.g. Santosh and Wada, 1993; Satish-Kumar, 2005). Thus, compilation of the carbon isotope data for graphite and fluid inclusions in coexisting minerals provides credible information both on the fluid source and on the thermal evolution of the fluid-rock system. These data can be compared with results obtained from conventional mineral thermometry (Santosh and Wada, 1993; Satish-Kumar, 2005).

The present paper reports data on mineralogy, bulk geochemistry, P-T-fluid conditions and carbon isotope composition of graphite and fluid inclusions in peraluminous garnet- and sillimanite-bearing granitoids associated with granulite metapelites from the Southern Marginal Zone (SMZ) of the Limpopo Complex, South Africa. We use the data to argue towards the external source of CO_2-rich fluids, which were transported by high-temperature (>900°) silicic magmas, and an origin for these magmas.

2. Geological setting, metamorphic evolution and granitoid magmatism of the Southern Marginal Zone of the Limpopo Complex

2.1. Tectonic structure and metamorphism

The high-grade metamorphic terrane of the Limpopo Complex is located between the Zimbabwe and the Kaapvaal cratons (Fig. 1*a*). The complex is subdivided into Northern Marginal Zone (NMZ), Central Zone (CZ), and Southern Marginal Zone (SMZ), which are separated by regional-scale shear zones. The CZ is a polymetamorphic terrane (e.g. Perchuk et al., 2008; Smit et al., 2011; Kramers and Zeh, 2011; Kramers et al., 2011; Kröner et al., 2018; Brandt et al., 2018) dominated by supracrustal lithologies. In contrast, the NMZ and SMZ are monometamorphic and considered to constitute the high-grade equivalents of the granite–greenstone successions of the adjacent cratons (Kreissig et al., 2000, 2001; Blenkinsop, 2011; van Reenen et al., 2011, 2014).

The SMZ is juxtaposed against the Northern Kaapvaal Craton along the shallow NE-dipping and SW-verging Hout River Shear Zone (HRSZ) in the south (Fig. 1*a*). This crustal-scale structure guided thrusting of the SMZ granulites onto the adjacent granite-greenstone terrane between ~2720 and 2690 Ma (Roering et al., 1992; Kreissig et al., 2001; van Reenen et al., 2011; Kramers et al., 2014; Smit et al., 2014). High-grade rocks of the SMZ occupy the hanging wall of the Hout River Shear Zone, while low-grade granite-greenstone lithologies of the Northern Kaapvaal Craton occupy the footwall (Fig. 1*a*). The SMZ comprises two major lithological units (e.g. van Reenen et al., 2011, 2014): (i) foliated and banded migmatized tonalitic-trondhjemitic Baviaanskloof Gneisses and (ii) Bandelierkop Formation - a sequence of ultramafic, mafic, pelitic and minor BIF granulites. These lithologies compose large crustal blocks displaying evidence of intense fold deformation bounded by steeply SW-verging regional scale high-grade shear zones (Annaskraal, Petronella, Matok) (Fig. 1*a*; Smit et al., 1992, 2014; Smit and van Reenen, 1997). Based on major, trace element, and Nd, Pb isotope data, Kreissig et al. (2000, 2001) concluded that the granulite facies rocks of the SMZ represent the high-grade equivalents of supracrustal rocks of the juxtaposed granite-greenstone terrane of the Pietersburg block of the Northern Kaapvaal Craton. This conclusion is supported by findings of detrital zircons with SHRIMP ages up to 3440 Ma in metapelites of the Bandelierkop formation (Rajesh et al., 2014), which are within the age span of adjacent sedimentary successions of the Kaapvaal Craton (e.g. Zeh et al., 2013). However, the Bandelierkop metapelites also contain abundant detrital zircons with ages <3000 Ma (Rajesh et al., 2014; Nicoli et al., 2015), which led Nicoli et al. (2015) to suggest that metasediments of the Bandelierkop Formation might not be related to the rocks of the Kaapvaal Craton, but belonged to an individual block colliding with the Kaapvaal Craton.

Ages of peak metamorphism of the rocks of the Bandelierkop Formation reported by various authors, i.e. 2717 ± 28 Ma (G.A. Belyanin et al., 2014), 2716 ± 6, 2718 ± 7 and 2714 ± 22 Ma (Rajesh et al., 2014), 2714 ± 6.4 and 2713 ± 5.4 Ma (Taylor et al., 2014), 2713 ± 8 Ma (Nicoli et al., 2015), are close to the ages of the metamorphic peak for the Baviaanskloof Gneiss (e.g. Retief et al., 1990) supporting the common metamorphic history of both major units in the SMZ. Conventional geothermobarometery and phase equilibria modeling applied by various groups of authors indicated peak metamorphic condition in the SMZ of 800–870 °C and 7.5–11 kbar (e.g., van Reenen, 1983; van Reenen et al., 1987; Stevens and van Reenen, 1992; Perchuk et al., 1996, 2000; Taylor et al., 2014; Nicoli et al., 2014, 2015). According to

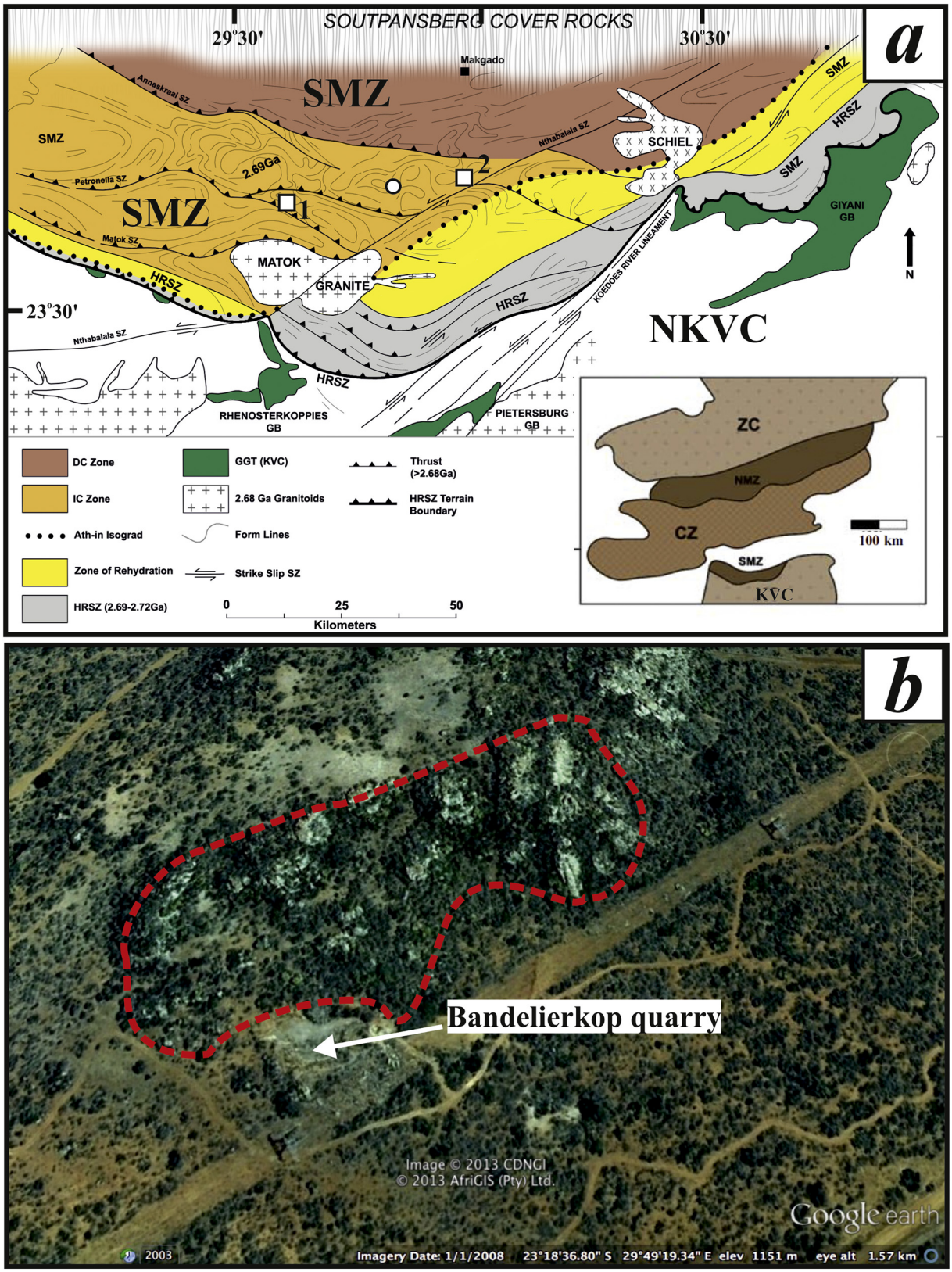

Fig. 1. Location of the studied area. (*a*) Geological map of the South Marginal Zone (SMZ) and adjacent Northern Kaapvaal Craton (NKVC) showing the location of the studied outcrop (white circle) at the Bandelierkop quarry (van Reenen, 1983; Stevens, 1991; Stevens and van Reenen, 1992; Taylor et al., 2014; Dubinina et al., 2015). White square (1) shows the locality of ca. 2.68 Ga trondhjemites at farm Petronella (Safonov et al., 2014; G.A. elyanin et al., 2014). White square (2) shows an approximate position of the locality of metapelites and leucocratic garnet-bearing pegmatoid trondhjemite described by Vennemann and Smith (1992). Abbreviations on the main figure: SZ – shear-zones, GB – greenstone belts, HRSZ – Hout River Shear Zone, Abbreviations on the inset figure: KVC – Kaapvaal Craton, CZ – Central Zone of the Limpopo Belt, NMZ – Northern Marginal Zone of the Limpopo Belt, ZC – Zimbabwe Craton. (*b*) Google Earth image showing the Bandelierkop quarry located immediately south of a large area characterized by masses of leucocratic granitoids (contoured by dashed line). Also outlined is the position of the large crosscutting granitoid body of this study that is located at the eastern entrance to the quarry (see Fig. 2*a*).

some authors (e.g., Stevens and van Reenen, 1992; Taylor et al., 2014; Nicoli et al., 2014, 2015), the peak metamorphic conditions have been attained via clockwise P–T evolution, reflecting burial of the rocks at the base of the continental crust and their prograde heating during collision. Based on Al-Opx + Sil + Qz, Opx + Crn, Spl + Qz (mineral abbreviations after Whitney and Evans, 2010) assemblages and anthiperthites, Tsunogae et al. (2004), Belyanin et al. (2010, 2012) and Rajesh et al. (2014) reported temperatures above 1000°C at 11–12 kbar in the Mg-Al-granulites of the SMZ. However, G. Belyanin et al. (2014) did not confirm these temperatures and pressures, but showed that the Mg-rich aluminous granulites of the SMZ still provide evidence for temperatures slightly above 900 °C, but at 6.5–7.0 kbar.

The post-peak metamorphic evolution of the SMZ between ~2720 and 2690 Ma reflects southwards thrusting of a hot allochtonous granulite nappe against and over the adjacent Kaapvaal Craton along the major SW-verging HRSZ shear zone (De Beer and Stettler, 1992; Roering et al., 1992; Smit et al., 1992, 2001, 2014; van Reenen et al., 2011, 2014). Granulites that outcrop north of the Annaskraal Shear Zone (DC zone in Fig. 1*a*) documents only evidence for decompression-cooling from ~870 °C at 8.3 kbar to ~600 °C at about 5 kbar (Perchuk et al., 1996, 2000; Smit et al., 2001, 2014; van Reenen et al., 2011, 2014). The age of the decompression-cooling stage, 2691 ± 7 Ma, has been obtained from monazites in metapelites showing common decompression-cooling reaction textures Grt + Qz = Opx + Crd (Kreissig et al., 2001). Rocks situated to the south of the Annaskraal shear zone (IC zone in Fig. 1*a*) document also evidence for near-isobaric cooling at 6.0–6.5 kbar. This stage is thoroughly recorded by the progress of the reaction Crd = Grt + Sil + Qz in metapelites (van Reenen, 1983; Stevens and van Reenen, 1992; Perchuk et al., 1996, 2000; Smit et al., 2001, 2014; Taylor et al., 2014; Nicoli et al., 2015; van Reenen et al., 2011, 2014; Safonov et al., 2014).

Sub-isobaric cooling in the SMZ was followed by regional retrograde hydration. This process established an "orthoamphibole isograd" (Fig. 1*a*; van Reenen, 1986; van Reenen et al., 2011, 2014; Smit et al., 2014; Koizumi et al., 2014), which is defined by the extensive formation of the assemblage Opx + Ath + Qz in metapelitic granulites south of the isograd (Fig. 1*a*). Rehydration of the SMZ rocks was controlled by complex CO_2-rich and aqueous brine fluids (van Reenen, 1986; van Reenen and Hollister, 1988; Baker et al., 1992; van den Berg and Huizenga, 2001; Huizenga et al., 2014; van Reenen et al., 2014). Most authors (van Reenen, 1986; van Reenen and Hollister, 1988; Smit et al., 2014; van Reenen et al., 2014; Koizumi et al., 2014; Kramers et al., 2014) agree that the source of these fluids was low-grade greenschists of the Kaapvaal craton buried underneath the granulites during thrusting of the SMZ against and over the adjacent Kaapvaal Craton. An alternative argument suggests that regional rehydration in the SMZ was caused by aqueous fluids that were released from crystallizing granitic magmas produced during prograde fluid-absent melting of metapelitic granulite, whereas CO_2 was produced in situ due to interaction of these fluids with graphitic material stored in metapelites (e.g. Stevens, 1997; Vennemann and Smith, 1992).

2.2. Granitoid magmatism

The metamorphic evolution of the SMZ was accompanied by complex anatexis (Du Toit et al., 1983; van Reenen et al., 2014; Taylor et al., 2014; Nicoli et al., 2015), which produced structurally different generations of peraluminous leucosomes (stromatic and nebulitic) with peritectic assemblages (Grt + Sil + Pl + Qtz, Opx + Grt + Pl + Qtz) in metapelites. In addition, the rocks of SMZ are intruded by various mainly undeformed post-tectonic granitoids. The largest is the syn-late-kinematic diorite-granodiorite-monzogranite Matok pluton with an age 2686 ± 7 Ma (Fig. 1*a*; Barton et al., 1992; Laurent et al., 2013, 2014; Laurent and Zeh, 2015), which was built both by the lithospheric mantle magmas interacted with subduction-related sedimentary material and magmas produced from the reworked crust (Laurent et al., 2014). A crustal origin is assigned to the Palmietfontein granite (2460–2450 Ma), which manifests the end of tectono-metamorphic activity related to the Neoarchean Limpopo event (Barton and Van Reenen, 1992).

The rocks of the SMZ are also intruded by smaller bodies of leucocratic granitoids, the origin of which is a matter of controversy. Kreissig et al. (2001) firstly obtained a Pb-Pb zircon evaporation age of 2643 ± 1 Ma from the wide granitic vein exposed in the Bandelierkop quarry (Fig. 1*a*) and interpreted this age to reflect the time of emplacement (crystallization) of leucocratic granitoids. Nicoli et al. (2015) recorded Pb-U ages of 2680 ± 6 Ma for homogeneous zircons from a crosscutting granitic pegmatite vein at the Brakspruit quarry (Fig. 1*a*) and concluded that this age corresponds to the age of crystallization of the granitic vein, but did not made any conclusion on the origin of this vein. G.A. Belyanin et al. (2014) reported an age of 2667 ± 9 Ma for zircon rims from a larger trondhjemite body at the Petronella locality (Fig. 1*a*) and also interpreted this as the age of trondhjemite emplacement. All ages obtained from crosscutting bodies are clearly lower that the peak metamorphic age (~2.72 Ga), in support of field evidence that these granitoids intruded already deformed and granulite-facies metamorphosed rocks. Based on the coincidence of these ages with the emplacement age of the Matok pluton, Safonov et al. (2014) and G.A. Belyanin et al. (2014) suggested that the trondhjemite bodies and veins could be satellites to the emplacement of the Matok pluton. Safonov et al. (2014) also showed that the joint cooling of the trondhjemite body and the contacting metapelites in the Petronella shear zone (Fig. 1*a*) occurred at pressures of about 6.0–6.5 kbar, which is consistent with the sub-sobaric cooling stage of the SMZ.

There is the bulk of evidence that, similar to the Matok magmas (e.g. Laurent et al., 2014; Laurent and Zeh, 2015), the leucocratic granitoids have been produced from a source unrelated to the Bandelierkop Formation. Based on $\delta^{18}O$ data obtained from a garnet-bearing pegmatitic trondhjemite vein, Vennemann and Smith (1992) also concluded that the trondhjemites were not in isotopic equilibrium with the adjacent metapelites but were crystallized from *melts being derived from several compositionally different but finely interlayered metasediments*. Based on a correlation of $\delta^{18}O$ with the composition of trondhjemites from the Banderlierkop quarry, Dubinina et al. (2015) also concluded that "the leucogranites represented partial melts derived from an external source and … were contaminated when they intruded the host metapelite".

Leucogranitic magmas also served as sources of fluids during the evolution of SMZ granulites. Stevens (1997) concluded that they carried essentially aqueous fluids (dissolved in magmas after the fluid-absent anatexis of mica-bearing metapelites), which participated in re-hydration of the SMZ metapelites at temperatures <650 °C and pressures 6.0–6.5 kbar. However, based on fluid inclusions in quartz and garnet in the trondhjemites and thermodynamic calculations, Safonov et al. (2014) showed that the magmas mainly carried CO_2-rich fluids of low water activity with lesser amounts of aqueous-salt bearing fluids. Another important indicator for the presence of carbonic fluids in the magmas is graphite (Vennemann and Smith, 1992). Graphite-bearing tonalites, trondhjemites and granites from the Bandelierkop quarry (Fig. 1*a*) are the focus of this study.

3. Field relations between graphite-bearing granitoids and host metapelites

The Bandelierkop quarry (23°18′36.80″ S; 29°49′19.34″ E) is located 3 km east of Bandelierkop village, south of the Annaskraal shear zone and about 8 km north of the anthophyllite-in isograd (Fig. 1). The quarry represents a seminal outcrop of migmatitic metapelites of the Bandelierkop Formation, which is one of the major supracrustal lithologies of the SMZ (Du Toit et al., 1983; van Reenen, 1983, 1986; Stevens, 1991; Stevens and van Reenen, 1992; Perchuk et al., 1996, 2000; van Reenen et al., 2011, 2014; Smit et al., 2014; Taylor et al., 2014; Safonov et al., 2014; Nicoli et al., 2015). Petrography, geochronology,

geochemistry and P-T data obtained from metapelitic granulites from this particular locality have been thoroughly highlighted in papers by van Reenen (1983), Stevens (1991), Stevens and van Reenen (1992), Kreissig et al. (2001), Taylor et al. (2014) and Dubinina et al. (2015). Three major varieties are distinguished among pelitic rocks exposed in the Banderlierkop quarry (van Reenen, 1983; Stevens and van Reenen, 1992; Taylor et al., 2014): (1) Grt-Opx (+Bt + Pl + Qz) semipelites, (2) Grt-Crd (+Bt + Pl + Qz) pelites, and (3) Crd-Opx (+Bt + Pl + Qz) pelites. Assemblages of these rocks, which are intermixed with leucosomes, reflect clear differences in bulk MgO/(MgO + FeO^T) ratio. Stevens (1991) and Stevens and van Reenen (1992) recognized five mineralogical types of peraluminous tonalite to granite leucosomes in the Bandelierkop quarry. Based on this, Taylor et al. (2014) grouped these leucosomes into two generations, i.e. stromatic and nebulitic, both containing peritectic phases (garnet, orthopyroxene, sillimanite). Stromatic leucosomes form veins, which are concordant with foliation of the host metapelites. They show internal fabric defined by elongated sillimanite crystals or stretched crystals of plagioclase and quartz. In contrast, less voluminous nebulitic leucosomes represent undeformed patches, which are superimposed on foliation of host rocks. They are interpreted to post-date the major deformation events in the locality (Taylor et al., 2014). Despite different position, both types of leucosomes showed the identical U-Pb zircon ages 2714 ± 6.4 and 2713 ± 5.4 Ma (Taylor et al., 2014).

In addition to these leucosomes, the Bandelierkop quarry also exposes a body of garnet-sillimanite-bearing granitoid, which contain

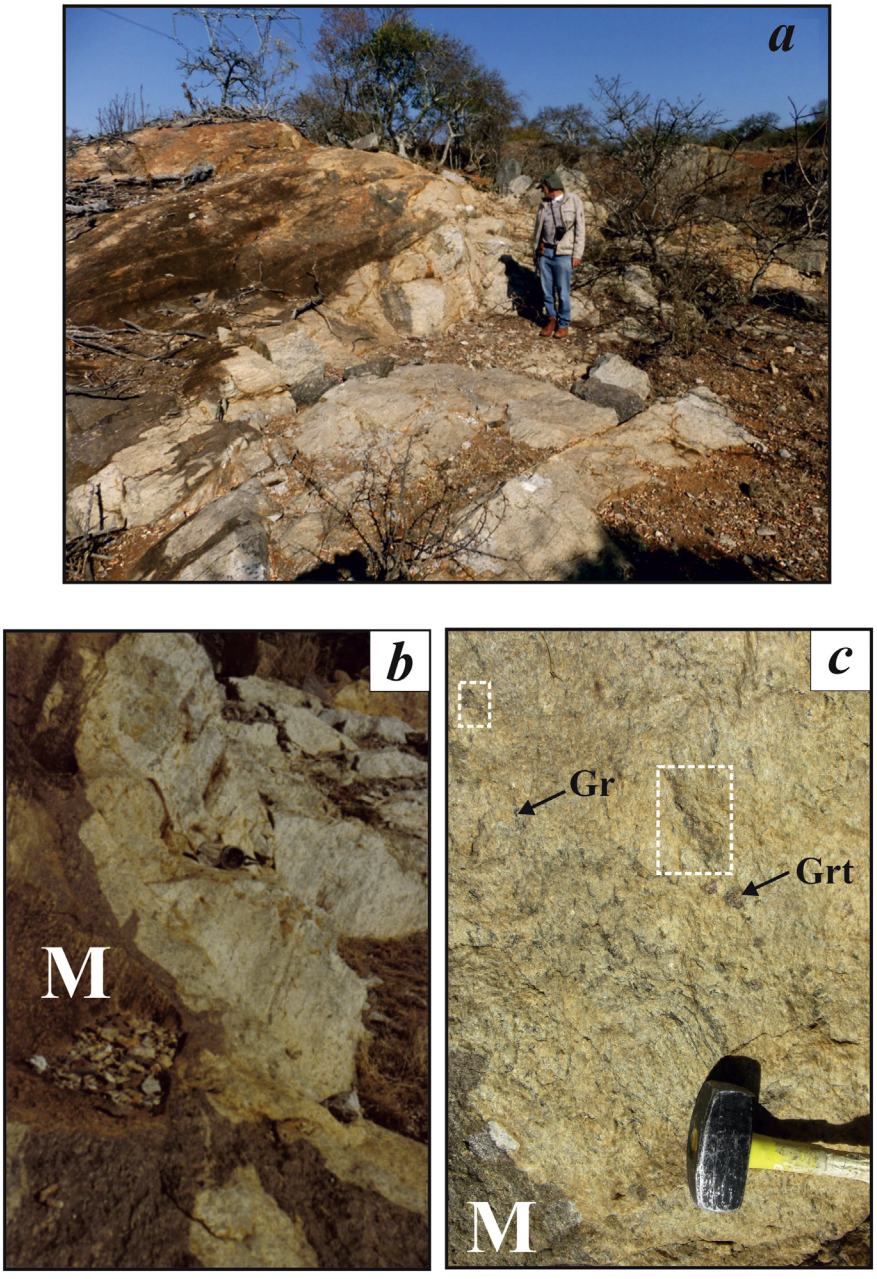

Fig. 2. Structural relations of the large crosscutting granitoid body with host metapelites at the eastern entrance to the Bandelierkop quarry. (*a*) A general view of the granitoid body at the entrance to the quarry (after van Reenen et al., 2014). Note the presence of partially assimilated metapelitic granulite. (*b*) Intrusive contact of the granitoid body (light colored) with metapelites (brown colored; M). (*c*) Internal mainly homogenous trexture of the granitoid close to the contact with metapelites. The sharp contact in the lower left corner between the leuco granitoid and metapelitic granulite (M) is plainly demonstrated. A weak foliation developed within the granitoids (panel *b*) is defined by stretched crystals of feldspar, quartz and aligned crystals of sillimanite and graphite, as well as by elongated metapelitic enclaves (white dashed boxes in panel *c*). (For interpretation of the references to color in this figure legend, the reader is referred to the web version of this article.)

accessory graphite. The outcrop of about 6 m-wide is located at the eastern entrance to the quarry (Figs. 1*a*, 2*a*, *b*) and shows massive medium to coarse-grained leucocratic rocks (Fig. 2*c*). The Google Earth satellite image (Fig. 1*b*) shows that the area directly north of Bandelierkop quarry is characterized by the presence of large irregular cluster of leucocratic granitoid bodies of which this particular outcrop is part of.

Contacts between the granitoids and host metapelites are sharp and oblique to the metapelite foliation (Fig. 2*b*, *c*). The granitoids contain small xenoliths of metapelites (Fig. 2*a*). Stretched crystals of feldspar, quartz and aligned crystals of sillimanite and graphite define the foliation developed within the granitoid body close to the contact with the metapelitic granulite (Fig. 2*b*). Closer examination also reveals the presence of semi-dissolved metapelitic enclaves, mostly defined by garnet and, probably also, cordierite grains mantled by mica-rich aggregates (Fig. 2*c*). Locally, these enclaves are attenuated along the foliation in the granitoids. The internal foliation of this granitoid body and the presence of attenuated metapelitic enclaves reflect evidence for a superimposed shear deformation (Du Toit et al., 1983), suggesting emplacement of the granitoid magmas during deformation.

4. Petrography, bulk rock characteristics and mineral assemblages of granitoids

4.1. Modal and bulk chemical composition

Garnet, sillimanite and graphite-bearing granitoids (i.e. rocks with >20 modal % of Qz; Le Maitre et al., 2002) of the Banderlierkop quarry (Table 1) are leucocratic medium to coarse-grained rocks consisting predominantly of plagioclase (50–70 vol%) and quartz (25–50 vol%). This mineralogical feature is reflected in their bulk composition: at the SiO_2 content 68–76 wt%, they usually show the CaO content above 1 wt%, a predominance of CaO + Na_2O over K_2O and $Na_2O/K_2O > 1$ (Table 2; Fig. 3*a*, *b*). In samples, where K-feldspar content is above 40% (samples L14-7-1 and L14-7-3; Table 2), the K_2O content is slightly higher than CaO + Na_2O, while Na_2O/K_2O is below unity. All granitoids are peraluminous with ASI > 1.1 (Fig. 3*c*). With respect to major element composition, the studied samples (L14-7-1 to L14-7-7 in Table 2) are very similar to granitoids from the Bandelierkop quarry described by Taylor et al. (2014) and Dubinina et al. (2015), as well as leucocratic granitoids associated with metapelites of the Bandelierkop formation (Stevens, 1997). However, granitoids have higher MgO + FeO content. It does not show correlation with the ASI index (Fig. 3*c*), which is typical for the S-type granitoids (e.g. Clemens et al., 2011). From the Ab-An-Or normative composition (Le Maitre et al., 2002) the most of granitoid rocks of the Bandelierkop quarry correspond to tonalites and trondhjemites (Fig. 4). However, some rocks (e.g. L14-7-1, SA-4-6A) are granites.

4.2. Mineralogy and petrographic features

K-feldspar is unequally distributed in the rocks (Table 1). In tonalites and trondhjemites, it occurs only as thin exsolution lamellae or coarse rectangular inclusions in plagioclase, as well as thin branchy rims at the plagioclase-quartz contacts. K-feldspar lamellae are usually concentrated in the centers of plagioclase crystals and clearly represent exsolution features from a ternary high-temperature phase rather than products of metasomatic replacement. In granites (L14-7-1, SA-4-6A; Tables 1 and 2; Fig. 5*a*), in addition to lamellae in plagioclase, K-feldspar forms coarse laminar textures with plagioclase (Fig. 5*a*). Coarsening of anthiperthite lamellae forming microveins, and the change in their orientation towards the periphery of the plagioclase crystals seems to reflect dissolution/precipitation during cooling in the presence of a fluid phase (e.g. Putnis, 2002). Individual grains of perthitic K-feldspar are also present in the rocks (Fig. 5*a*). Textures of the K-feldspar-rich varieties closely resemble textural features of hypersolvus granitoids (e.g. Tuttle and Bowen, 1958).

Garnet is a major Fe-Mg mineral, although its content is below 1–2 vol% (Table 1). It occurs as separate or accreted irregular or rounded garnet grains with sizes from 0.2–0.5 up to 4–5 mm (Fig. 5*a*, *b*, *d*) that are dispersed in the quartz-feldspathic matrix. Garnet grain margins are predominantly clear and only some grains are rimmed by thin K-feldspar veins. Rare biotite fringes appear at the garnet contacts with K-feldspar or anthiperthitic plagioclase. Taylor et al. (2014) also noted that the dominant variety of subhedral to rounded garnet in the intrusive granitoid body is predominantly inclusion-free and shows no evidence of retrogression. However, some garnets contain inclusions of quartz, rutile, zircon, monazite, and apatite (Fig. 5*b*). Inclusions of plagioclase, sillimanite and graphite are rare, although garnet is closely associated with these phases (Fig. 5*a*, *b*). Inclusions of spinel were found in garnets of the sample L14-7-1. K-feldspar has not been observed as inclusion in garnet in any of the studied samples.

Sillimanite in some samples (Table 1) forms large (up to 500 μm) disoriented crystals in the quartzo-feldspathic matrix (Fig. 5*a*, *c*, *d*) and is closely associated with garnet in sample L14-7-1 (Fig. 5*a*). In other samples, sillimanite forms elongated lens-like aggregates (Fig. 5*c*, *d*). Individual flakes of biotite are extremely rare in the studied granitoids.

Common accessory phases in the tonalites, trondhjemites and granites are zircon, apatite, monazite, rutile and pyrite (Table 1). Rutile is main Ti-bearing accessory phase in the rocks and is found both in the matrix and as inclusions in garnets. Ilmenite was observed only in one sample (SA-4-6A), where it is partially surrounded by rutile at the

Table 2
Bulk composition of leucocratic granitoids from the Bandelierkop quarry.

Sample	SA-4-6A	L14-7-1	L14-7-4	L14-7-5	L14-7-6	L14-7-7
SiO_2	69.24	68.95	72.98	71.79	75.63	67.7
TiO_2	0.07	0.03	0.03	0.47	0.00	0.13
Al_2O_3	17.78	16.11	15.45	14.78	15.73	18.63
Fe_2O_3	0.80	3.16	1.62	3.94	2.1	1.89
MnO	0.01	0.00	0.00	0.00	0.05	0.00
MgO	0.18	1.06	0.31	1.33	0.69	1.44
CaO	1.86	0.69	0.95	2.11	1.26	3.49
Na_2O	5.47	3.22	3.67	4.19	2.65	4.15
K_2O	3.1	5.36	3.85	1.01	1.50	1.19
P_2O_5	0.12	0.09	0.06	0.15	0.00	0.07

Note. Sample SA-4-6A is described in the paper by Dubinina et al. (2015).

Table 1
Mineral assemblages of the studied granitoids from the Bandelierkop quarry.

Sample	Pl	Qtz	Kfs	Grt	Sil	Bt	Ru	Ilm	Gph	Mnz	Zrc	Spl	Crd	Sulfides	Secondary
L14-7-1	+, i	+, i	p, l, cl, r	+	+	−	+, i	−	+		+	i	−	Pyr	Cal, Ap, Mu, Ab, Brt
L14-7-4	+	+	l, r	+, e	+, e	e		−	+	e	+	e, i	−	Po [e], Cpy [e], Pyr [e]	Mu, Bt
L14-7-5	+	+, i	l, r	+	−	−	+, i	−	+	+		−	−		Bt
L14-7-6	+	+, i	p, l, r	+	+	−		−	+, i		i	−	−		Cal, Chl, Mu, Ap
L14-7-7	+	+, i	l, r	+, e	e	e	i	−		i, e		−	e	Pyr	Mu, Bt, Cal, Chl
SA-4-6A	+	+	p, l, cl, r	+	−	−	+	+	+			−	−	Pyr, Cpy	Chl, Ab

+ - mineral is present in the rock matrix; − - mineral is absent; K-feldspar: p – individual perthitic K-feldspar grains, l – lamellae in plagioclase, cl – coarse lamellae intergrowths with plagioclase, r – rims around plagioclase; i – inclusions in garnet; e – in miceous enclaves. Empty cells mean that mineral is, probably, present, but was not identified during microprobe and BSE examination.

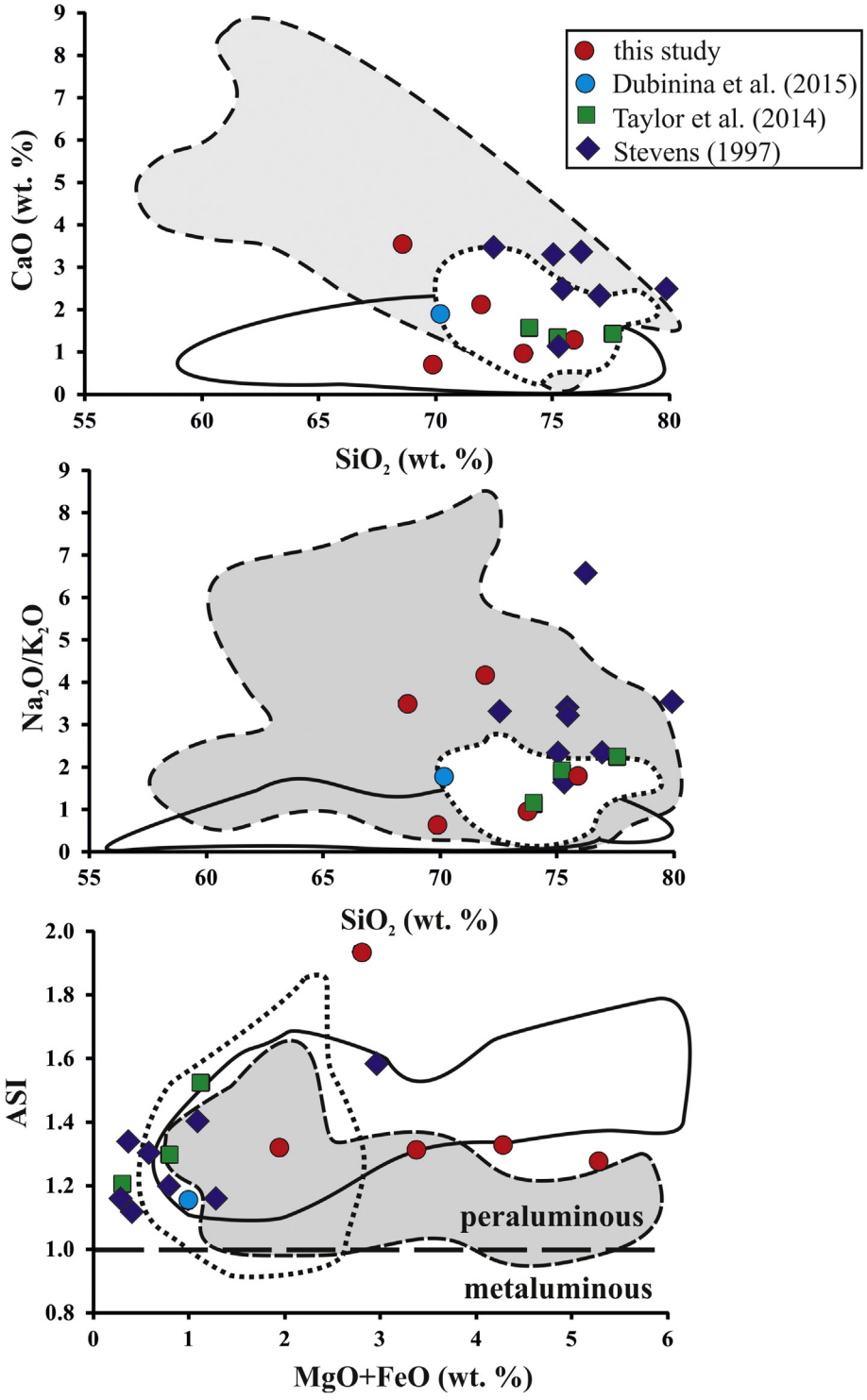

Fig. 3. Major element compositional characteristics of the granitic samples from the Bandelierkop quarry described in this paper (Table 1). (*a*) SiO_2 - CaO content (wt%) binary diagram; (*b*) SiO_2 – Na_2O/K_2O (wt%) binary diagram; (*c*) (MgO + FeO) – ASI index binary diagram, ASI = mol. $Al_2O_3/(K_2O + Na_2O + CaO)$. Field countered by the solid line shows the compositions of melts produced in various experiments on melting of metapelites (Le Breton and Thompson, 1988; Vielzeuf and Holloway, 1988; Patiño Douce and Johnston, 1991; Pickering and Johnston, 1998; Patiño Douce and Harris, 1998; Koester et al., 2002). The grey field with dashed boundaries contours compositions of melts produced in various experiments on melting of amphibolites (Beard and Lofgren, 1991; Rapp et al., 1991; Rushmer, 1991; Wolf and Wyllie, 1994; Patiño Douce and Beard, 1995; Skjerlie and Patino Douce, 1995; Sisson et al., 2005; Clemens et al., 2006). The field countered by the dotted line shows compositions of melts produced in various experiments on melting of tonalites (Skjerlie and Johnston, 1993; Patino Douce, 1997; Gardien et al., 2000; Watkins et al., 2007). Long-dashed line at ASI = 1.0 in panel *c* defines the boundary between peraluminous and metaluminous granitoids.

contact with the feldspathic matrix. Zircon, apatite and monazite are found both in the quartzo-feldspathic matrix of granitoids and as inclusions in garnet. In contrast to surrounding metapelites, no pyrrhotite is observed in the rocks. Pyrite (accompanied locally by chalcopyrite) is a common sulfide in the trondhjemites and granites (Fig. 5*f*), while small inclusions of native gold associated with pyrite were found in plagioclases of the sample SA-4-6A.

The modal proportion of graphite in the granitoids does not exceed 1 vol%. It usually forms flakes of sizes from 100–200 μm to several mm in the quartzo-feldspathic matrix of the rocks where it is closely

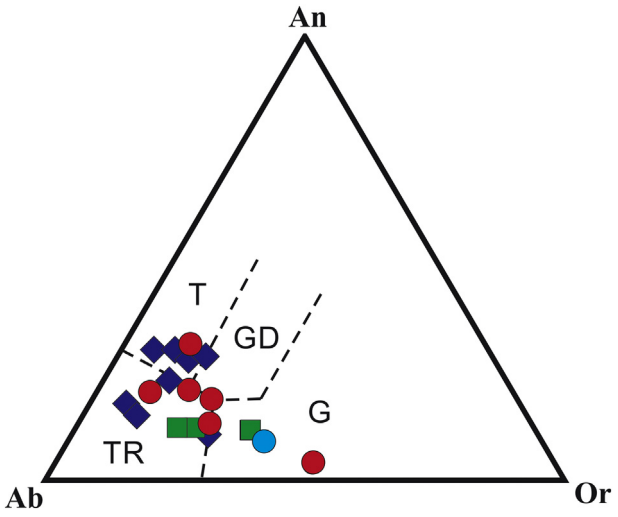

Fig. 4. Normative Ab-An-Or composition of granitoid samples from the Bandelierkop quarry, Southern Marginal Zone, Limpopo Complex, described in this paper. Markers are the same as in Fig. 1*a–c*. G – granite, GD – granodiorite, T – tonalite, TR – trondhjemite.

associated with garnet, plagioclase, K-feldspar, sillimanite and rutile (Fig. 5*b*, *c*, *d*, *f*). It also forms rare tiny inclusions in garnet and intergrowths with sillimanite (Fig. 5*b*, *c*). Graphite also occurs as flakes along feldspar and quartz grain boundaries, but some flakes are totally included in both homogeneous and antiperthitic varieties of plagioclase (Fig. 5*c*, *d*, *f*). In some portions of the rock, graphite flakes mark boundaries of the biotite-garnet and biotite-cordierite-garnet metapelite enclaves (see below; Fig. 5*d*). Locally, graphite is associated with pyrite (Fig. 5*f*).

Granitoids show evidence for extensive late alteration (Table 1) in which chlorite and Ti-poor (or Ti-free) biotite are locally riming garnets grains or developed in cracks in garnet. Locally, primary sillimanite is partially replaced by muscovite (and diaspore) at the contacts with K-feldspar or antiperthitic plagioclase in the granitic matrix. Chlorite and muscovite are extensively developed in the micaceous enclaves, where their aggregates replace biotite. Pyrite grains in the granitic matrix are locally strongly oxidized to limonite and are accompanied by a network of thin veinlets of Sr-bearing barite, which is also found as separate grains locally associated with armenite $BaCa_2Al_6Si_9O_{30}\cdot 2(H_2O)$ and albite that formed at the expense of Ba-bearing K-feldspar. Tiny grains of apatite and allanite are associated with the late minerals. Carbonates (mostly, calcite) fill cracks in garnet and plagioclase grains.

4.3. Micaceous enclaves in granitoids

Although primary biotite is rare in the studied samples, the trondhjemite samples L14-7-4 and L14-7-7 (Tables 1 and 2), contain spectacular biotite-bearing enclaves of various sizes (up to several tens of mm) (Fig. 5*d*). The enclaves are aggregates of biotite with sillimanite and quartz, which locally preserve relics of garnet, cordierite and plagioclase (Fig. 5*d*, *e*). Garnet and cordierite are usually resorbed by Ti-poor biotite or biotite-sillimanite-quartz aggregates (Fig. 5*e*). In contrast to garnets in the quartz-feldspathic matrix of the rocks, garnets in the micaceous enclaves contain inclusions of plagioclase and biotite along with inclusions of quartz. Late subhedral garnets with numerous inclusions of sillimanite and quartz are developed along the contacts of large garnet grains with relict cordierite (Fig. 5*e*), while veinlets of acicular and fibrous sillimanite fill cracks in the relict cordierite and plagioclase grains. These textural features are very similar to widespread textures observed in metapelites of the SMZ (including metapelites of the Banderlierkop quarry), which are interpreted as products of various reactions (e.g. Crd = Grt + Sil + Qz) during near-isobaric cooling (van Reenen, 1983; Perchuk et al., 1996, 2000; Stevens, 1997; Smit et al., 2001; van Reenen et al., 2011; Safonov et al., 2014). The enclaves contain pyrrhotite and pentlandite, which are characteristic for metapelites, but are not observed in the granitoids. In contrast to surrounding metapelites, the enclaves are much strongly retrogressed, as is reflected by extensive development of chlorite, muscovite, carbonates etc.

5. Mineral chemical characteristics

5.1. Garnet

Representative analyses of garnets from the studied samples are presented in Table S1. Two compositional types of garnet are distinguished in the studied granitoids: (1) garnets that are dispersed in the quartz-feldsparthic matrix of the rocks and unrelated to the garnet-biotite and garnet-cordierite-biotite enclaves (Fig. 5*a*, *b*, *d*), and (2) garnets in the enclaves (Fig. 5*d*, *e*). In the sample L14-7-1, garnet coexisting with sillimanite (Fig. 5*a*) is slightly zoned with respect to X_{Ca}, which increases from 0.015 to 0.019 towards the garnet rims at constant X_{Mg} about 0.29 (Fig. 6; Table S1). Garnets that do not coexist with sillimanite (samples L14-7-4, L14-7-5, L14-7-6), show higher X_{Ca} (0.017–0.034), while their X_{Mg} values in cores vary from 0.38 to 0.43 for different garnet grains (Fig. 6; Table S1). No zoning with respect of X_{Mg} and X_{Ca} is observed within cores. However, X_{Mg} decreases at the garnet rims by 0.07–0.11 at constant X_{Ca}. Two varieties of garnet distinguished by Taylor et al. (2014) in the intrusive granitoid body show X_{Mg} = 0.33–0.35 and X_{Ca} about 0.02 in the cores and X_{Mg} = 0.28–0.33 and X_{Ca} = 0.02 at the rims, which is within the compositional range of garnets in our samples (Fig. 6).

Garnets restricted to the micaceous enclaves show variable X_{Mg} and X_{Ca} values (Fig. 6; Table S1). They are more calcic than the garnets not associated with the enclaves (X_{Ca} = 0.02–0.05), but show comparable X_{Mg} values in their cores (Fig. 6). At rims, garnets in the enclaves are strongly zoned with respect to X_{Mg}, which drops in some cases below 0.30 (Fig. 6; Table S1). Texturally, these Fe-enriched rims are in contact with late biotite (locally, chloritized) or biotite + sillimanite aggregates.

A comparison of the compositions of garnets from granitoids with the composition of garnets from host metapelites (Fig. 6) clearly indicates that garnets in the micaceous enclaves are relics phases from garnet-cordierite-biotite metapelites. Significantly, no garnets with compositions comparable to garnets of the garnet-orthopyroxene semipelites are observed in granitoids (Fig. 6). Strong variations in X_{Mg} of garnets from the enclaves are related to extensive Fe-Mg exchange during late re-hydration. Following from their X_{Mg} and X_{Ca} values, garnets in the quartzo-feldspathic matrix of granites are also relics of garnets from metapelites. However, they clearly show lower X_{Ca} that implies a probable re-equilibration with the plagioclase-rich granitoids. Garnets coexisting with sillimanite in granite L14-7-1 (Fig. 5*a*) seem to represent a separate generation, probably, unrelated to metapelites.

5.2. Biotite

Primary biotite is absent in the granitoids, but occur as relics in the garnet-biotite and garnet-cordierite-biotite enclaves (Fig. 5*d*, *e*). Rare inclusion in garnets and relatively large flakes (usually surrounded by later aggregates of biotite + sillimanite + quartz) show X_{Mg} = 0.75–0.78 and 4.0–4.4 wt% TiO_2 (Table S2 in Supplementary material). These values are similar to those obtained from biotites from garnet-cordierite-biotite metapelites of the Bandelierkop quarry. Biotites associated with sillimanite and quartz in the micaceous enclaves show X_{Mg} = 0.69–0.79, whereas the TiO_2 contents vary from 3.8 to below detection limit without any clear correlation with the Mg-number (Table S2 in Supplementary material). Higher TiO_2 concentrations, probably, belong to relics of earlier biotite. A unique biotite was found associated with the late garnet-sillimanite-quartz textures developing after cordierite in micaceous enclaves in granitoid of the sample L14-7-7 (Fig. 5*e*). Being less magnesian (X_{Mg} = 0.69–0.72) with widely varying, but generally low TiO_2 content (0–2.6 wt% TiO_2), this biotite is characterized

by 1.5–2.1 wt% Cl (Table S2 in Supplementary material). Such biotite has not been identified in metapelites. The composition of biotite fringes around some garnet grains in granitoids is similar to that of late biotite in the micaceous enclaves. In general, compositions of late biotites in granitoids and in micaceous enclaves are comparable to compositions of late biotite in metapelites, suggesting that they originated during a single fluid-rock interaction event.

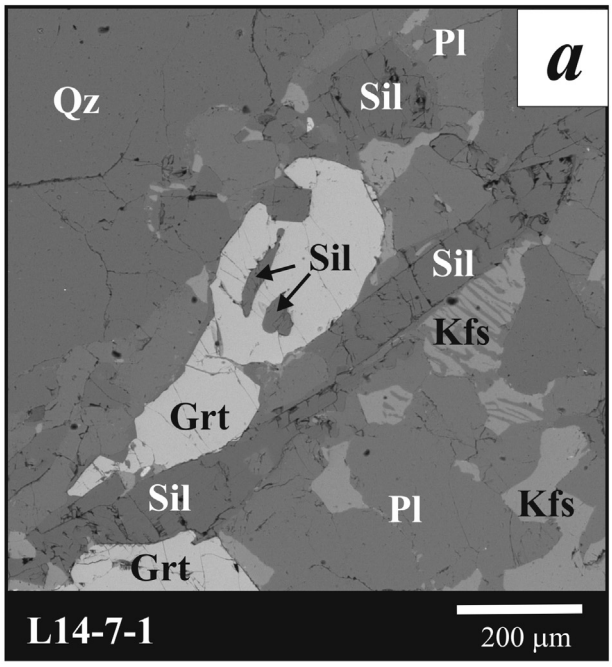

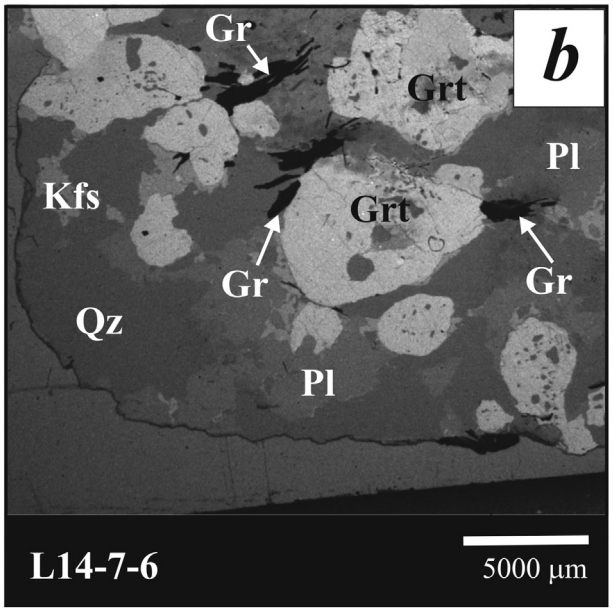

Fig. 5. . Textural and mineralogical characteristics of the studied granitoids from the Bandelierkop quarry (Table 1). (*a*) Accreted garnet grains associated with large sillimanite crystals in the granitic sample L14-7-1 (Table 1); note, K-feldspar forms coarse grains along the plagioclase and plagioclase-quartz grain boundaries, as well as separate coarsely exsolved grains. (*b*) Large garnet grains associated with graphite in the sillimanite-free trondhjemite L14-7-6 (Table 1). (*c*) Sheaf-like lense of sillimanite in quartz-plagiocalse matrix of the trondhjemite L14-7-4 (Table 1); note that graphite is intergrown with sillimanite. (*d*) Biotite-garnet enclave in the trondhjemite L14-7-4; graphite is developed along grain boundaries and also outlines the enclave. (*e*) Close view of garnet from the metapelite enclave in the trondhjemite L14-7-7; garnet contain inclusions of quartz, plagioclase and biotite; at contacts with cordierite it is rimmed by new garnet-sillimanite intergrowths; matrix of the enclave is extensively replaced by biotite-sillimanite-quartz aggregates. (*f*) Pyrite associated with graphite in hypersolvus granite SA-4-6A.

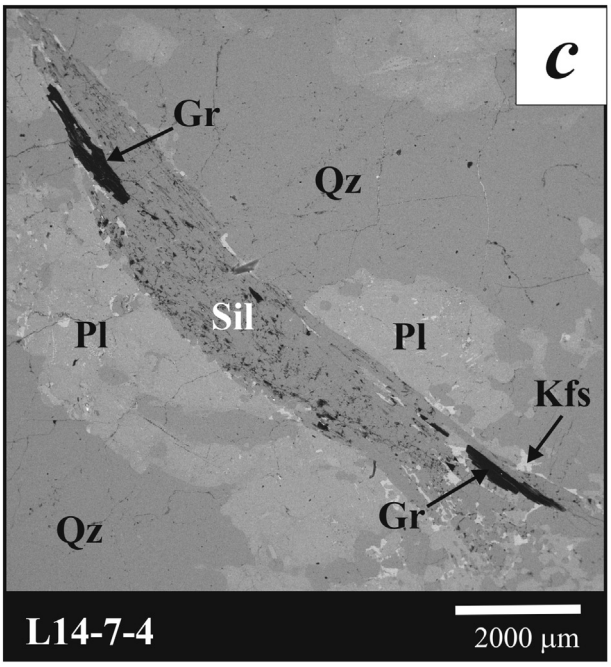

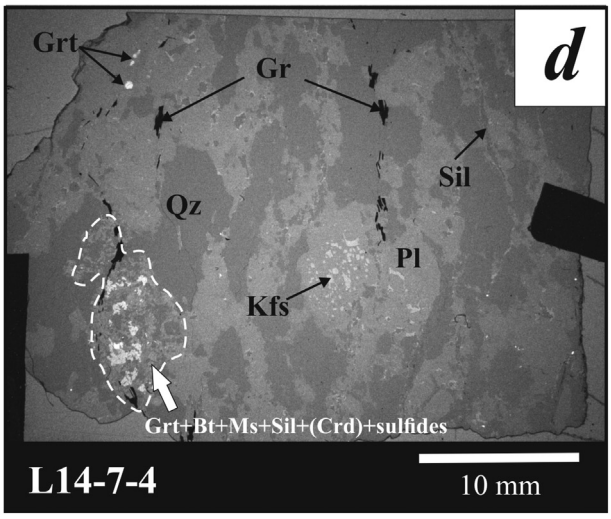

Fig. 5 (*continued*).

5.3. Cordierite

The X_{Mg} values (0.85–0.89) in cordierite from micaceous enclaves in the sample L14-7-7 (Table 1) are similar to those of cordierites from the surrounding metapelites. Usually, X_{Mg} of cordierite either decreases by 2–4 mol.% or remains constant towards contacts with late garnet-sillimanite-biotite-quartz developing after cordierite.

5.4. Spinel

Spinel inclusions in garnets from the trondhjemite L14-7-1 (Table 1) show $X_{Mg} = 0.41–0.44$, are free of Cr_2O_3, but contain 4.9–5.9 wt% ZnO. Small spinel inclusions were identified in garnet from the micaceous enclave in the sample L14-7-4 (Table 1). It is more magnesian ($X_{Mg} = 0.54$), Cr-free and contains about 3 wt% ZnO.

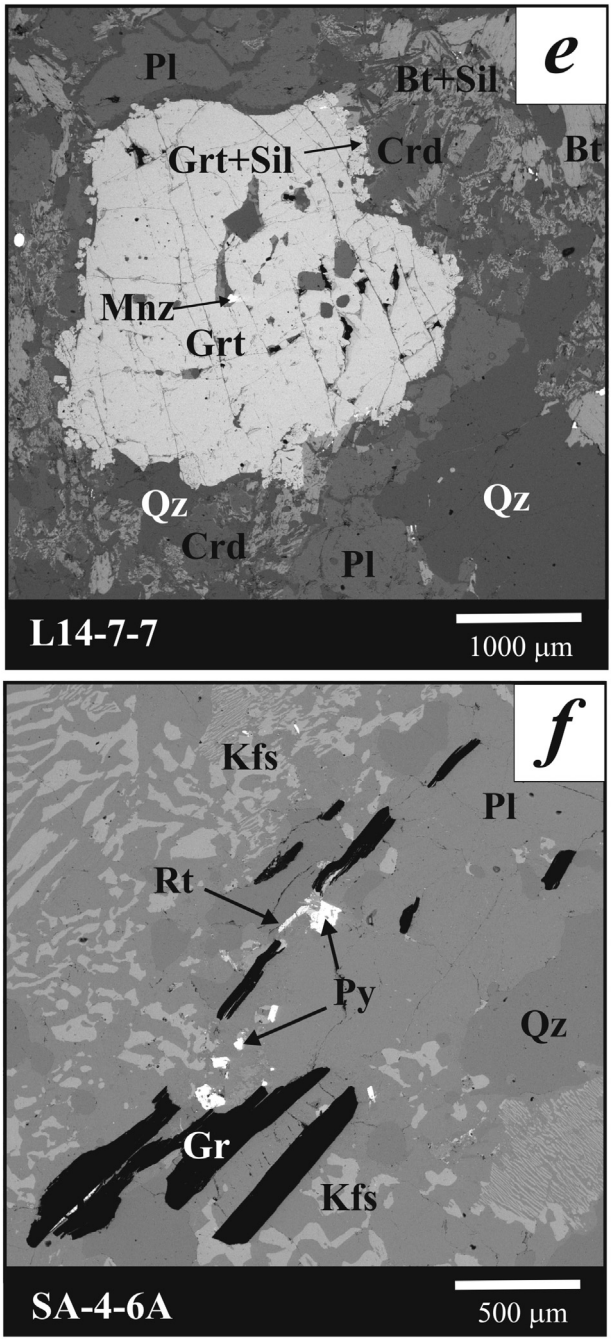

Fig. 5 (*continued*).

5.5. Plagioclase, K-feldspar and ternary feldspars

Plagioclase in trondhjemites and granites can be subdivided into two compositional groups. The first group includes large plagioclase grains containing rare thin K-feldspar lamellae or is devoid of them. Plagioclases without K-feldspar lamellae show X_{An} = 0.19–0.23 (rarely up to 0.25) and X_{Or} varying within 0.012–0.031. Re-integrated compositions of exsolved plagioclases using a rastered electron beam show X_{An} = 0.18–0.22, but their measured X_{Or} values are 0.08–0.25 (mean value is about 0.15) (Fig. 7; Table S3 in Supplementary material). The second group consists of plagioclases intergrown with coarse K-feldspar representing re-crystallized laminar textures of two minerals. This plagioclase is more sodic, X_{An} = 0.15–0.17, and shows X_{Or} = 0.003–0.015.

Plagioclases from the biotite-garnet and biotite-cordierite-garnet enclaves in granitoids are distinctly more calcic, X_{An} = 0.31–0.35, and show X_{Or} predominantly below 0.015. This composition is analogous to the composition of plagioclases from garnet-cordierite-biotite and orthopyroxene-cordierite-biotite metapelites of the Bandelierkop quarry (X_{An} = 0.32–0.38, X_{Or} = 0.002–0.015), but differs from plagioclases of the orthopyroxene-garnet semipelites (X_{An} = 0.50–0.53, X_{Or} = 0.006–0.015). This is one more indication that the biotite-garnet and biotite-cordierite-garnet enclaves in granites are remnants of the surrounding metapelites.

Re-integrated compositions of perthitic alkali feldspar from various granitoid samples show two groups of feldspars (Fig. 7; Table S3 in Supplementary material): (1) X_{Or} = 0.33–0.40, X_{Ab} = 0.51–0.57 and X_{An} = 0.07–0.11 (close to the anorthoclase field) and (2) X_{Or} = 0.55–0.67, X_{Ab} = 0.27–0.37 and X_{An} = 0.04–0.08. Feldspars of both groups coexist in the sample L14-7-1.

5.6. Accessory minerals

The specific feature of monazite in granitoids is an elevated content of ThO_2. Usually, it is 3.5–4.9 wt%, but grains with up to 15 wt% ThO_2 were identified in the micaceous enclaves being closely associated with late biotite, chlorite and muscovite (Table 1). Rare primary apatite inclusions in garnet contain about 1.2 wt% F with only traces of Cl. In contrast, apatite associated with late assemblages shows up to 0.4 wt% Cl at about 0.8 wt% F. Pyrite in the granitoids contains 0.1–0.2 wt% Co and Ni. This Co and Ni concentrations are very similar to those observed in the later pyrite in metapelites, which develops after pyrrhotite and pentlandite. Pyrrhotite in granitoids is observed within the micaceous enclaves suggesting its relict origin. The Fe/S atomic ratio in pyrrhotite varies from 0.90 to 0.94, whereas concentrations of Ni and Co reach 0.8 and 0.5 wt%, respectively. This composition is close to the pyrrhotite composition in metapelites.

6. Graphite characteristics and carbon isotope composition

Although Stevens (1991) has previously mentioned graphite in the leucosomes of the Bandelierkop quarry, he provided no detailed characterization of this mineral. It is well known that the degree of ordering of carboniferous matter is directly dependent on the metamorphic grade (e.g. Beyssac et al., 2002 and references therein), and that this feature can be characterized using Raman spectroscopy and the X-ray diffraction pattern of graphite. Raman spectra of graphite from the granitoids were obtained on double-polished sections used for the fluid inclusion study. Taking into account that the thin-section fabrication during the polishing stage can induce severe damages to the graphite structure, measurements were performed by focusing the laser beam on graphite flakes beneath the surface of a transparent quartz, as have been recommended by Pasteris (1989) and Beyssac et al. (2002). Fig. 8*a* shows two first-order Raman spectra obtained for graphite from the sample L14-7-1, taken both for the surface of a graphite flake and for a flake from underneath the surface of quartz. Both spectra show intense G-band at 1582 cm^{-1}. However, the spectrum taken from the graphite surface shows an intense and relatively wide band D1 at 1345 cm^{-1} and shoulder D2 at 1624 cm^{-1} that is assigned to defects in the graphitic structure suggesting a high degree of disordering (e.g. Tuinstra and Koenig, 1970). The D1 and D2 bands are absent in the spectrum taken from a flake from underneath quartz that is indicative of high degree of atomic ordering and crystallinity along the basal plane in the graphite structure. Following to the conclusion by Beyssac et al. (2002) on the negative correlation between the R2 = D1/(G + D1 + D2) (where D1, D2, G – band areas) ratio with the metamorphic temperature, the ratio R2 = 0 that characterises the second spectrum corresponds to highly ordered graphite formed at temperatures above 650 °C. This conclusion is supported by the parameter c = 6.7084 ± 0.0002 Å and d_{002} = 3.35347 Å obtained from the X-ray pattern (Fig. 8*b*), that corresponds to ordered

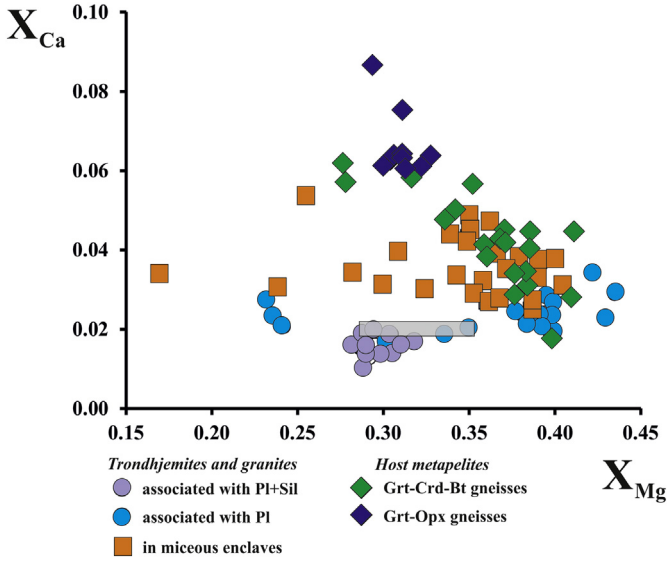

Fig. 6. Compositional characteristics of garnets of granitoids in comparison to garnets from host garnet-cordierite and garnet-orthopyroxene metapelites of the Bandelierkop quarry. Grey box shows a range of garnet composition measured by Taylor et al. (2014).

graphite crystallized above 720 °C (Shengelia et al., 1979; Luque et al., 1993).

The carbon isotope composition of graphite was measured for samples L14-7-1, L14-7-4 and L14-7-5 (Table 3). Variations of $\delta^{13}C_{PDB}$ for individual samples are 0.02–1.2‰. The $\delta^{13}C_{PDB}$ values for graphite from the samples L14-7-4 and L14-7-1 are practically similar, whereas they are about 2‰ "heavier" for graphite from the sample L14-7-5.

7. Fluid inclusions characteristics and carbon isotope composition

CO_2 is the prevailing type of fluid inclusions in granitoids of the Bandelierkop quarry and was identified both in quartz and garnet. Sample SA-4-6A (Tables 1 and 2) contains three distinct textural groups of CO_2 inclusions (Fig. 9*a*–*d*). The first group involves primary inclusions, which form isolated clusters in centers of quartz grains (Fig. 9*a*). Usually, these are small (5–15 μm) isometric inclusions with discernable faces. Inclusions with size up to 25 μm are less common. Primary inclusions in quartz show densities 1.087–1.071 g/cm^3, homogenization temperatures down to −32.6 °C (Fig. 9*d*) and melting temperatures varying from −57.8 °C to −58.3 °C. Inclusion of the second group mark healed fractures (Fig. 9*b*), which do not transect grain boundaries (pseudosecondary inclusions). Size of the pseudosecondary inclusions does not exceed 10–15 μm. They are less dense (1.06–0.91 g/cm^3), show melting temperatures from −57.3 °C to −58.7 °C and a wide range of homogenization temperatures (Fig. 9*d*). Pseudosecondary carbonic inclusions in garnet of sample SA-4-6A are elongated, worm-like or hook-like in shape, with stretched ends (Fig. 9*c*). Densities of the pseudosecondary inclusions in garnet vary within 0.86–0.85 g/cm^3. Their homogenization temperatures are above 5 °C (Fig. 9*d*) and melting temperatures vary from −58.9 to −59.2 °C.

Carbonic inclusions in minerals of the sample SA-4-6A show distinctly lower melting temperatures with respect to pure CO_2 (−56.6 °C) suggesting the presence of CH_4 in the inclusions (e.g. van den Kerkhof and Thiéry, 2001). Lower density pseudosecondary inclusions in quartz and garnet usually show lower melting temperatures in comparison to the primary inclusion in quartz. Following to diagrams by van den Kerkhof and Thiéry (2001), the CH_4 content in the primary inclusions varies within 5–7 mol.%, but increases up to 10 mol.% in the pseudosecondary inclusions in quartz. The CH_4 mol.% is up to 15 mol.% in the pseudosecondary inclusions in garnet of the sample SA-4-6A.

Measurable primary carbonic inclusions were not identified in samples L14-7-4, L14-7-5 and L14-7-6, while common pseudosecondary carbonic inclusions are usually localized along healed cracks in quartz. In the sample L14-7-4, inclusions are light, no larger than 15 μm in size, round, with sharp boundaries. Rare inclusions with sizes up to 20 μm and a negative crystal shape are present. The homogenization temperature and density of carbonic inclusions vary from −40.4 to 29.1 °C and from 1.118 to 0.627 g/cm^3. The melting temperatures of these inclusions, from −57.1 to −58.1 °C, indicate a presence of about 5 mol.% of CH_4 (van den Kerkhof and Thiéry, 2001). In the sample L14-7-5, small (5–10 μm) isometric inclusions, in some cases, with discernable faces show the temperatures of homogenization from −41.5 °C to +27.8 °C and densities from 1.122 to 0.66 g/cm^3. The melting temperature of these inclusions ranging from −57.3 to −56.8 °C suggests 2–3 mol.% of CH_4. The melting temperature of the carbonic inclusions in sample L14-7-6 from −57.1 to −56.7 °C corresponds to even lower CH_4 content (1–2 mol.%). These inclusions are usually no >5–10 μm (rarely up to 15–20 μm), are isometric or negative crystal in shape. The homogenization temperatures and density ranged from −42.1 to 28 °C and 1.125 to 0.655 g/cm^3, respectively.

Following to the melting temperatures, carbonic inclusions in all studied samples contain CH_4 (van den Kerkhof and Thiéry, 2001). Raman spectra of pseudosecondary inclusions revealed that CH_4 (main band at 2917 cm^{-1}; Frezzotti et al., 2012) was the most common species in the carbonic inclusions from the samples SA-4-6A, L14-7-4, L14-7-5 and L14-7-6 (Fig. 10*a*). In addition to CH_4 bands, Raman spectra of inclusions from the samples L14-7-4, L14-7-5 and L14-7-6 also show wide bands at ~1580 and ~1350 cm^{-1} (Fig. 10*a*), attributed to carboniferous matter (graphite). Rare inclusions show presence of water (very wide band between 3100 and 3600 cm^{-1} in Raman spectra). Methane and carboniferous matter are notably less abundant or absent in the primary high-density carbonic inclusions in the sample SA-4-6A (see lower graph in Fig. 10*a*).

Aqueous-salt inclusions were not identified in the sample SA-4-6. In samples L14-7-4, L14-7-5 and L14-7-6, the pseudosecondary carbonic inclusions are associated with pseudosecondary aqueous-salt inclusions. Aqueous-salt inclusions are strongly subordinate. They are light, irregular in shape, with sizes <20 μm. Because of size, initial melting of the inclusions is hard to measure precisely. For larger inclusions, it is observed at temperatures from −58 to −53 °C, which are close to the eutectic melting of ice + hydrohalite + antarcticite and suggest a

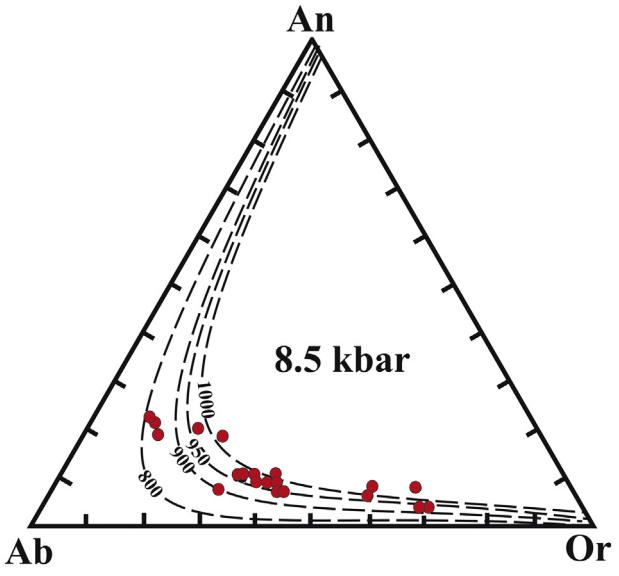

Fig. 7. Reintegrated compositions of exsolved plagioclases and alkali feldspars in trondhjemites and granititoids plotted on isotherms in the system Ab-An-Or calculated from the ternary feldspar model of Elkins and Grove (1990).

presence of NaCl and $CaCl_2$ in the solution (e.g. Steele-MacInnis et al., 2011). Final melting temperature in order to determine salinity is hard to obtain. Some aqueous-salt inclusions contain small bubble. Raman spectra of such inclusions show a band of CH_4 (Fig. 10*b*).

All studied samples contain relatively large (20–30 μm) aqueous inclusions of irregular, amoeba-like shape. They are localized in healed fractures. The instantaneous melting temperature varies from −1 to −0.1 °C suggesting almost pure water without salt. This fluid, likely, represents a late meteoric fluid.

As for graphite, the carbon isotope composition of the gas phase of fluid inclusions was measured for samples L14-7-1, L14-7-4 and L14-7-5 (Table 3). Fluid extracted from the inclusions in the sample L14-7-5 also shows "heavier" $\delta^{13}C_{PDB}$ values with respect to other samples. In addition, we have measured $\delta^{13}C_{PDB}$ for fluid extracted from thin leucocratic veins in the host metaplite (sample SA-4-5 in Table 3), which gave a value −5.04‰.

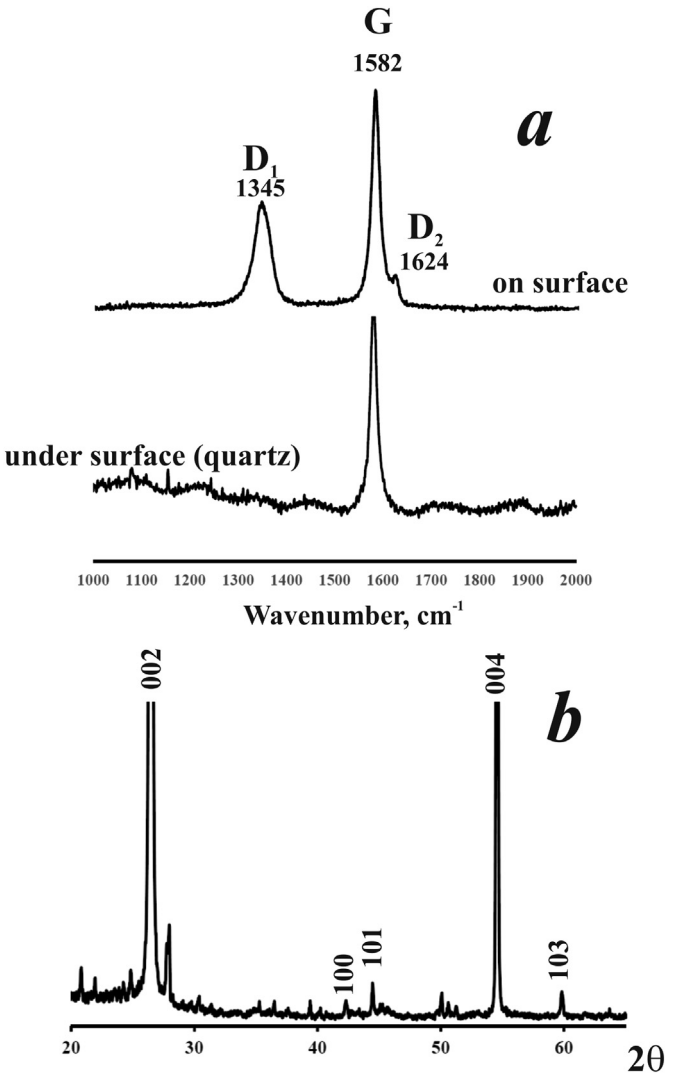

Fig. 8. Graphite characteristics. (*a*) Raman spectra taken for graphite flakes (sample L14-7-1) on the polished surface (upper spectrum) and graphite plunged into quartz (lower spectrum); G, D_1 and D_2 – major first-order bands of graphite (e.g. Tuinstra and Koenig, 1970). (*b*) XRD pattern for graphite from the sample L14-7-1.

8. P-T conditions of the crystallization of granitoids

8.1. Conventional thermobarometry

Granitoids of the Bandelierkop quarry do not contain assemblages of Mg-Fe minerals suitable for temperature calculations. The only approach to estimate temperatures of granite crystallization is to use re-integrated compositions of antiperthite plagioclases and perthite alkali feldspars from the rocks. Fig. 7 compares these compositions with isotherms in the ternary system albite-orthoclase-anorthite calculated via equations by Elkins and Grove (1990) for a pressure of 8.5 kbar (see below). Despite a wide variation of the feldspar composition with respect to the albite component, the data points are well accommodated between the isotherms 800–1000 °C with a statistical peak (n = 20) at about 920 °C.

A pressure marker for granitoids is the assemblage garnet + sillimanite + plagioclase + quartz that is, for example, observed in the sample L14-7-1 (Fig. 5*a*). Garnet from this sample is considered to be a product of direct crystallization from the granitic melt. Fig. 11 shows lines for the equilibrium

$$\text{Grs (in Grt)} + 2\text{Sil} + \text{Qz} = 3\text{An (in Pl)} \quad (1)$$

calculated for several values of the grossular contents in garnets coexisting with sillimanite, plagioclase and quartz from the sample L14-7-1, using the winTWQ (version 2.32) software (Berman, 2007) with end-member mineral thermodynamic properties according to Berman (1988) and a solid solution model for garnet from Berman and Aranovich (1996). For temperature intervals above 900 °C these equilibrium lines together with the CO_2 isochores (calculated using EOS by Sterner and Pitzer, 1994) confine the pressures between 7.5 and 9.5 kbar (Fig. 10). Accounting for Fe^{3+} in garnet (0.05–0.2 a.p.f.u. for garnets from different samples; see Table S1 in Supplementary materials) results in displacement of the reaction (1) by only about 0.5 kbar to lower pressure.

Cooling of the granitoids is reflected in only slight variations of X_{Ca} in garnet at almost constant X_{Mg}. In some garnets, which do not coexist with sillimanite, the cooling stage is reflected in a decrease of X_{Mg}. The cooling stage is best evident in the biotite-cordierite-garnet enclaves within the granites. Some garnets in the enclaves are strongly zoned with X_{Mg} decreasing towards rims. The cooling is expressed in the formation of the garnet-sillimanite-quartz textures surrounding earlier relict garnet and the extensive formation of biotite (+sillimanite + quartz) in the enclaves. The Mg-Fe exchange equilibrium between garnet and cordierite in the vicinity of the garnet-sillimanite textures gives temperature values of 560–580 °C, whereas the Mg-Fe exchange equilibrium between garnet and biotite show a range of temperatures 600–630 °C.

8.2. Phase equilibria modeling of granitoid crystallization

Mineralogical data, fluid inclusions and re-integrated composition of feldspars indicate that the crystallization of granitoids at the

Table 3
Average (of *n* individual measurements) $\delta^{13}C_{PDB}$ values for graphite and fluid extracted from the fluid inclusions in quartz from granitoids and metapelite of the Bandelierkop quarry.

Sample	$\delta^{13}C^{Gr}_{PDB}$	$\delta^{13}C^{fluid}_{PDB}$	Δ
L14-7-5	−6.52 (*n* = 3)	−2.50 (*n* = 3)	4.02
L14–7-4	−8.65 (*n* = 2)	−4.22 (*n* = 2)	4.43
L14-7-1	−8.59 (*n* = 2)	−5.58 (*n* = 2)	3.01
SA-4-5	–	−5.04 (*n* = 3)	–
V6D[a]	−6.40	–	–

[a] Graphite from the garnet trondhjemite vein described by Vennemann and Smith (1992).

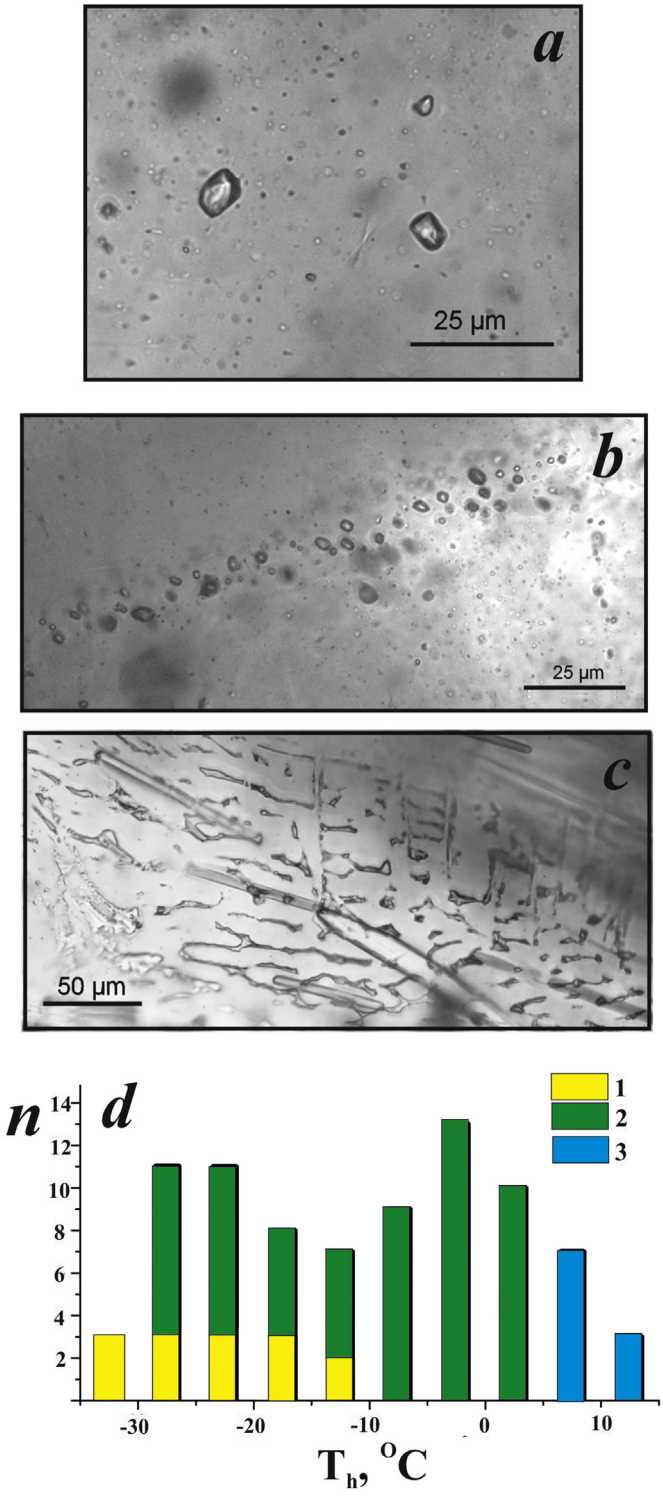

Fig. 9. Fluid inclusions in the granite SA-4-6A. (*a*) Isolated primary carbonic inclusions in quartz. (*b*) Trails of pseudosecondary carbonic inclusions healing fracture in quartz. (*c*) Pseudosecondary carbonic inclusions in garnet. (*d*) Histogram of the homogenization temperatures of carbonic inclusions: 1 – primary inclusions in quartz, 2 – pseudosecondary inclusions in quartz, 3 – pseudosecondary inclusions in garnet.

Bandelierkop quarry occurred at pressures between 7.5–9.5 kbar and temperatures >900 °C in the presence of CO_2-bearing fluid. In order to model the mineral assemblages forming during crystallization of the granitoids and to demonstrate a dependence of these assemblages on bulk composition of the granitoids, T-X_{CO2} pseudosections have been constructed for a mean pressure 8 kbar for bulk compositions of the samples L14-7-1, L14-7-5 and L14-7-7 (Table 2).

We applied phase equilibria modeling for specific bulk composition based on Gibbs free energy minimization in the system MnO–Na_2O–CaO–K_2O–FeO–MgO–Al_2O_3–SiO_2–H_2O–TiO_2–O_2 (MnNCKFMASHTO) using the PERPLE_X software (Connolly, 2005) in version 6.7.7 for Windows. The updated standard properties database hp11ver.dat (i.e. Holland and Powell, 2011) and solution model database solution_model.dat (http://www.perplex.ethz.ch) were applied for modeling. The following models from White et al. (2014) were applied for mineral and melt solutions (see descriptions at http://www.perplex.ethz.ch/perplex/datafiles/solution_model.dat): "Gt(W)" for Fe^{3+}-bearing Ca-Mg-Fe-Mn garnet, "Bi(W)" for Ti and Fe^{3+}-bearing biotite and "Mica(W)" for white mica. The model "feldspar" based on the solution model of Fuhrman and Lindsley (1988) was taken for ternary feldspar. The model melt(W) from White et al. (2014) was used for the NCKFMASH silicate melt. The T-X_{CO2} pseudosections were constructed assuming saturation of the system with the H_2O-CO_2 fluid with variable X_{CO2}. The "free" O_2 (which serves as a monitor of Fe_2O_3) content 0.001 wt% was taken arbitrarily based on following prepositions. Garnet containing relatively low Fe^{3+} concentrations (Table S1) is the only principle Fe^{3+}-bearing phase in the granitoids. Its low modal content (<5%) impose low Fe^{3+} content in the rock bulk composition. Rutile rather than ilmenite is stable the granitoids. Calculations of the T-M_{O2} (where M_{O2} is a content of "free" O_2 in the system) pseudosection for the bulk composition of the sample L14-7-1 at 8 kbar and $X_{CO2} = 0.7$ (see Fig. S1 in Supplementary materials) shows that ilmenite appears in the assemblage Grt + Pl + Kfs + Sil + Qz at M_{O2} just above 0.002 wt% without any critical influence on the composition of garnet. Stability of pyrite instead of pyrrhotite in the granitoids also imply low Fe_2O_3 (i.e. "free" O_2) content in the rocks.

Crystallization of the granitoids begins with garnet and rutile and is followed by quartz and plagioclase (Fig. 12*a*–*c*). K-feldspar coexists with melts only at the solidi of the K_2O-rich sample L14-7-1 (Table 2). In the samples L14-7-5 and L14-7-7 (Fig. 12*b*, *c*), K-feldspar appears exclusively in the sub-solidus region via exsolution from plagioclase solid solution on cooling. All these features are consistent with the petrographic observations. Solidi temperatures for all samples are extremely dependent on X_{CO2}, increasing from 650 to 710 °C at $X_{CO2} = 0$ up to 1000 °C at $X_{CO2} = 0.8$–0.9. The hypersolvus appearance of the rocks indicates that ternary feldspars crystallized at the solidus and were exsolved at under sub-solidus conditions. The pseudosections indicate that such sequence of mineral crystallization is possible at $X_{CO2} > 0.6$ for the sample L14-7-5 (Fig. 12*b*) and at $X_{CO2} > 0.7$ for the samples L14-7-7 and L14-7-1 (Fig. 12*a*, *c*), respectively. At these X_{CO2} conditions, solidus temperatures of the granitoids are above 800 °C, i.e. at temperatures close to the peak metamorphic temperatures deduced for the metapelites of the Bandelierkop Formation (e.g., van Reenen, 1983; Stevens and van Reenen, 1992; Perchuk et al., 1996, 2000; Taylor et al., 2014; Nicoli et al., 2014, 2015). The subsolidus assemblage is Grt + Pl + Qz + Sil + Rt. However, the sillimanite content predicted for the sample L14-7-5 is below 0.3 vol%. A sillimanite content above 2 vol% is predicted for the sample L14-7-1, which is consistent with the presence of this phase both in the matrix and as inclusions in garnet in the sample (Fig. 5*a*). Saturation of the sample L14-7-7 with sillimanite corresponds to the presence of the sillimanite-bearing micaceous metapelite enclaves in the sample (Fig. 5*e*). At the above X_{CO2}, biotite appears only in the subsolidus region on cooling, reflecting the absence (or extreme rarity) of the biotite-forming back reactions in the studied granitoids. Pseudosections (Fig. 12*a*–*c*) adequately reproduce compositions of garnets in the studied samples indicating lower grossular content of garnet in the granitoid L14-7-1 in comparison to garnets in the samples L14-7-5 and L14-7-7 (Fig. 6). All pseudosections indicate formation of carbonates at temperatures about 600 °C at $X_{CO2} > 0.9$. This result is consistent with the presence of carbonate veinlets along cracks in plagioclase and garnets and supports the conclusion on the action of the CO_2-rich fluid down to lowest temperatures.

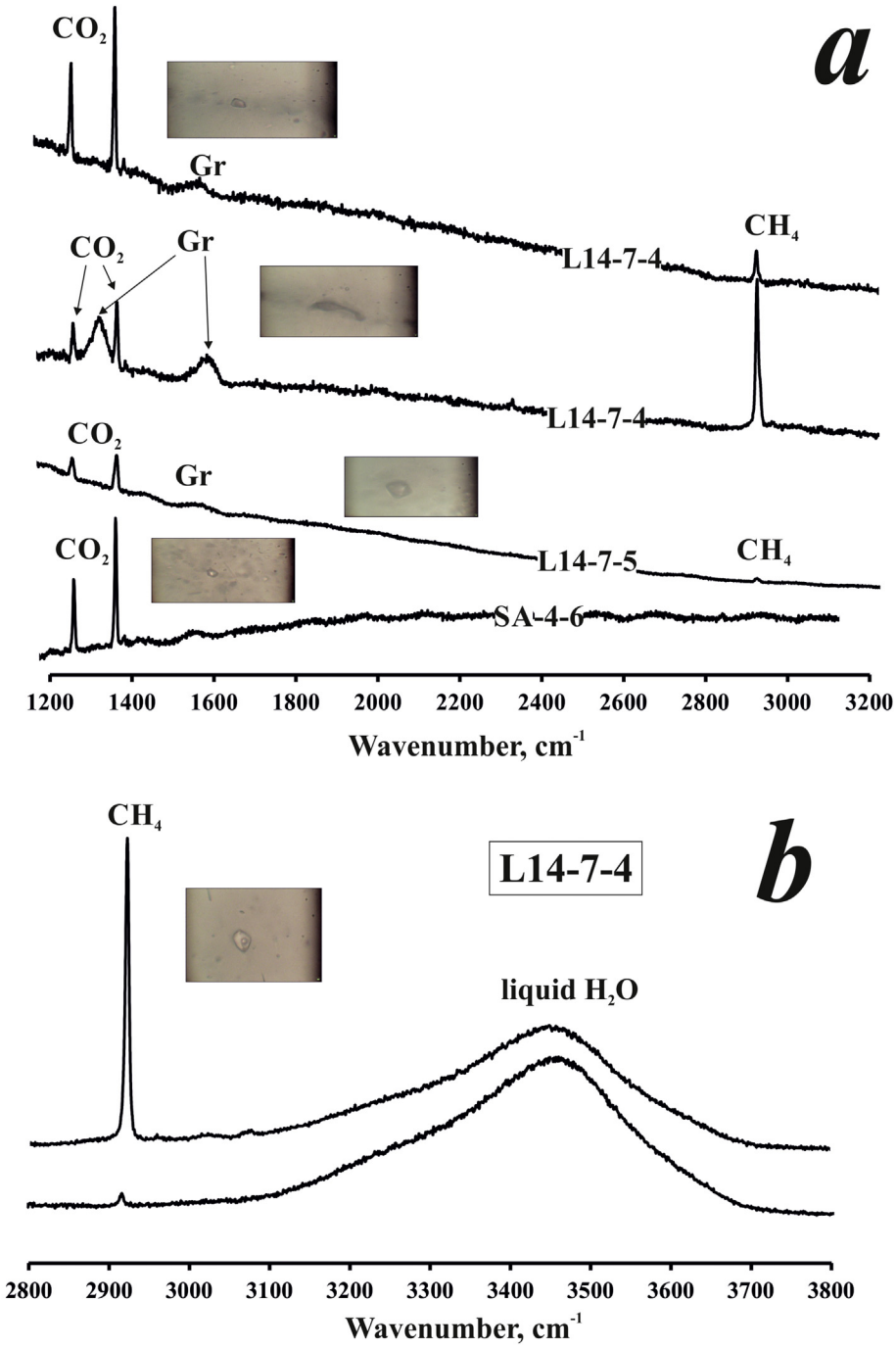

Fig. 10. Raman spectra of fluid inclusions in the granitoids. (*a*) Spectra of carbonic inclusions in quartz from the samples L14-7-4, L14-7-5 and SA-4-6 showing various contents of CH_4 and graphite substances; lower graph shows spectrum of an isolated primary inclusion in quartz from sample SA-4-6A. (*b*) Spectrum of aqueous inclusion in quartz from the sample L14-7-4 showing variable contents of CH_4. Bands are assigned after Frezzotti et al. (2012).

The pseudosection for the sample L14-7-7 (Fig. 12*c*) shows stability of cordierite-bearing assemblages at $X_{CO2} < 0.2$. Cordierite disappears on cooling giving place to the assemblage Grt + Bt + Sil + Qz. Muscovite joins the assemblage on cooling in this portion of the diagram. Thus, the pseudosection at $X_{CO2} < 0.25$ closely reproduces mineral assemblages of the micaceous enclaves, which are abundant in the sample L14-7-7 (Fig. 5*e*). It describes the local decrease of the X_{CO2} in the fluid as a result of dissolution of the H_2O-rich metapelite relics in the granitoid magma that stabilized hydrous minerals over a wide temperature range.

In order to further specify P-T conditions for the trondhjemites, we have calculated the P-T pseudosection (Fig. 13*a*) and corresponding isopleths for garnet and plagioclase (Fig. 13*b*) for the sample L14-7-5 at $X_{CO2} = 0.7$. The P-T pseudosection demonstrates that the sequence of mineral crystallization does not significantly depends on pressure. Within the pressure interval 4–10 kbar, cooling of the magma results in primary crystallization of garnet and rutile followed by ternary feldspar and quartz. Sillimanite joins the assemblage close to the solidus, which is rather independent on pressure. Exsolution of feldspar occurs under sub-solidus conditions. Biotite and low-temperature muscovite appear deep within the subsolidus region if the H_2O-CO_2 fluid is still present in the system. The best convergence of isopleths of the pyrope content in garnet 40–42 mol.% and the anorthite content of plagioclase 19–22 mol.% (Tables S1 and S3) is observed within the pressure interval

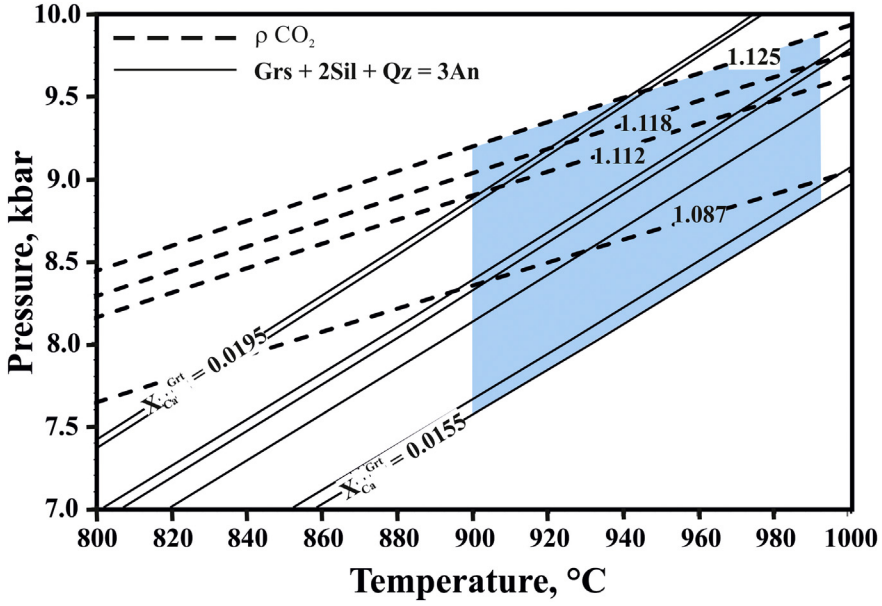

Fig. 11. P-T diagram showing lines of the equilibrium (1) calculated for compositions of garnet and plagioclase coexisting with sillimanite and quartz (solid lines) and CO_2 isochores (dashed lines) for inclusions in the trondhjemite L14-7-1 calculated using EOS for CO_2 after Sterner and Pitzer (1994). Blue field covers possible P-T conditions for the trondhjemite crystallization. (For interpretation of the references to color in this figure legend, the reader is referred to the web version of this article.)

7–9 kbar and temperatures 900–930 °C (Fig. 13*b*). This is consistent with the ternary feldspar thermometry (Fig. 7) and fluid inclusion densities (Fig. 11).

9. Discussion

9.1. Fluids in the granitoids

Carbonic fluid inclusions in quartz and garnet from tonalites, trondhjemites and granites revealed that CO_2 was a predominant component of fluids that accompanied the granitoid magmas during their intrusion into the Bandelierkop metapelites. Pseudosection modeling of mineral assemblages of the granitoids further proves the hypersolvus nature of the rocks, the absence of primary biotite and shows that back reactions of garnet + K-feldspar with melt or fluid to biotite are possible only at X_{CO2} above ~0.6 (Fig. 12*a–c*). The presence of graphite and late carbonates as veinlets in the minerals implies that CO_2 was active during the entire cooling evolution of the granitoids.

The characteristic component of the carbonic fluid inclusions is methane, which, according to Raman analyses (Fig. 10*a*, *b*). The presence of methane, as well as carboniferous matter in some fluid inclusion (Fig. 10*a*, *b*), further indicates that the fluid, which accompanied granitoids during their emplacement into metapelites, was not originally pure CO_2, but contained H_2O (e.g. Hollister, 1990) and coexisted with graphite due to the equilibrium

$$2C + 2H_2O = CO_2 + CH_4 \quad (2)$$

(e.g. Whitney, 1992; Giorgetti et al., 1996). This equilibrium allows calculation of the composition of the C-O-H fluid within the temperature interval 950–800 °C at 8 kbar at fixed $X_O = O/(O + H)$. We used $X_O = 0.6$ corresponding to $X_{CO2} = 0.5$, which is a minimum X_{CO2} in a fluid coexisting with the assemblage Grt + Pl + Kfs + Sil + Qz estimated from pseudosections (Fig. 12*a–c*). Using the fluid EOS by Zhang and Duan (2009) (implemented in the Excel spreadsheet GFluid; Zhang and Duan, 2010) we obtained that the fluid contained 46.6–48.7 mol.% H_2O, 49.0–49.9 mol.% CO_2, 2.8–0.7 mol.% CO, 0.9–0.4 mol.% CH_4, and 0.7–0.2 mol.% H_2.

Coexistence of the fluid with graphite is further testified by the relation $\delta^{13}C_{PDB}^{Gr} < \delta^{13}C_{PDB}^{fluid}$ for three samples (Table 3). The higher $\delta^{13}C_{PDB}^{fluid}$ corresponds to higher $\delta^{13}C_{PDB}^{Gr}$ value in sample L14-7-5, while the lower $\delta^{13}C_{PDB}^{fluid}$ corresponds to lower $\delta^{13}C_{PDB}^{Gr}$ value in sample L14-7-1 (Table 3). These relations are consistent with the case of near-equilibrium fractionation between graphite and CO_2 fluid (Bottinga, 1969; Friedman and O'Neil, 1977; Scheele and Hoefs, 1992; Polyakov and Kharlashina, 1995), while variations in $\delta^{13}C_{PDB}$ from lower to higher values can be caused by Rayleigh-type fractionation during cooling (e.g. Satish-Kumar, 2005). In this case, the closure temperatures of the isotope exchange would determine the isotope fractionation between graphite and CO_2 from the inclusions (e.g. Santosh and Wada, 1993; Satish-Kumar, 2005). In order to estimate these temperatures, we have calculated fractionation values $\Delta_{CO2\text{-graphite}}$ from average $\delta^{13}C_{PDB}$ values for graphite and fluid inclusions from quartz (Table 3), which are 4.0 (from 2.3 to 5.8) for the sample L14-7-5, 4.4 (from 4.0 to 4.8) for the sample L14-7-4 and 3.0 (from 2.7 to 3.3) for the sample L14-7-1. A curve for the fractionation between CO_2 and graphite plotted on the basis of the β-factors for CO_2 and graphite from the paper by Polyakov and Kharlashina (1995) gives the following temperature intervals: 956–1115 °C for the sample L14-7-4, 1288–1465 °C for the sample L14-7-1 and 824–1638 °C for the sample L14-7-5 (Fig. 14). The temperature range calculated for the sample L14-7-4 and lower estimates for the sample L14-7-5 are close to the temperature values obtained from the feldspar solvus (Fig. 7) supporting high temperatures crystallization of the studied granitoids. Nevertheless, the calculated values vary widely and many of them are unrealistically high, reflecting the fact that present values do not represent true equilibrium. There are several reasons for overvalued temperatures determined from the isotope fractionation. First of all, the presence of CH_4 and carboniferous matter in the inclusions does not preclude the late re-equilibration of, at least, some inclusions and displacement of the $\delta^{13}C_{PDB}$ for CO_2. The applied approach of comparing the bulk (averaged) compositions of the fluid and graphite for the determination of the fractionation factor

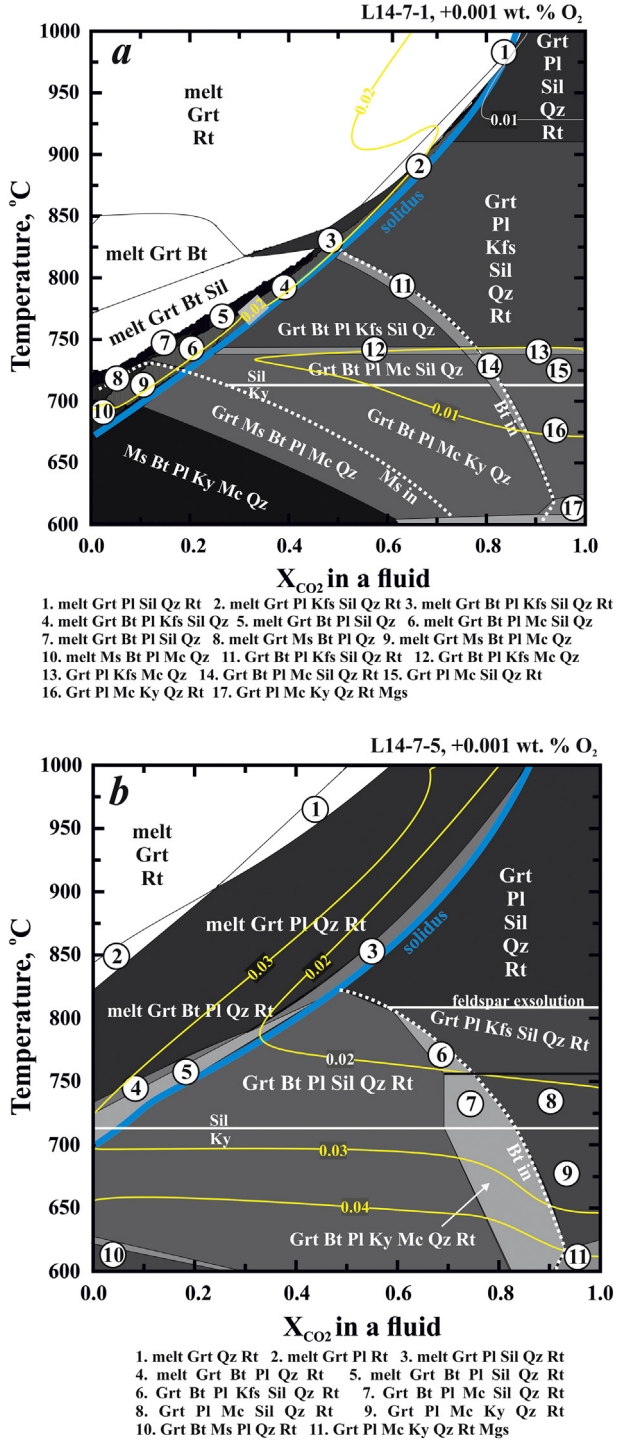

Fig. 12. T-X_{CO2} pseudosections computed for bulk compositions of the samples L14-7-1 (*a*), L14-7-5 (*b*) and L14-7-7 (*c*) at pressure 8 kbar. Blue lines mark the solidi of the rocks, while dotted lines show the appearance of biotite and muscovite. Yellow lines are X_{Ca} isopleths of garnet. Bulk compositions are shown in Table 2. (For interpretation of the references to color in this figure legend, the reader is referred to the web version of this article.)

balanced, to some extent, the influence of local effects, but significantly promotes errors of the temperature estimation, which are reflected in the obtained wide temperature intervals. Another factor, which surely could influence the isotope fractionation, is contamination of the magmatic fluids by the metapelitic carbon, which includes both dispersed carbon (e.g. Vennemann and Smith, 1992; Stevens, 1997) and CO_2 in cordierite.

In addition to the CO_2-rich aqueous-carbonic fluid, granitoids also carried the aqueous-salt fluid preserved as pseudosecondary inclusions in quartz. The aqueous-salt fluid fraction seemed to have appeared at the latest stages as a result of accumulation of water and salt components during crystallization of the magma and escape of CO_2. The action of the aqueous-salt fluids is expressed in formation of late Cl-enriched (0.4 wt% Cl) apatite and biotite. It cannot be excluded that formation of K-feldspar microveins along the plagioclase-quartz contacts in the granitoids (Fig. 5*a–d*) were locally related to the action of the late salt-rich fluid (cf. Aranovich and Safonov, 2018; Aranovich, 2017). Coupled with $X_{Mg} = 0.69–0.72$, the concentrations 1.5–2.1 wt% Cl in biotite correspond to extremely high Cl content in the coexisting fluid (Munoz and Swenson, 1981; Zhu and Sverjensky, 1992; Aranovich and Safonov, 2018; Aranovich, 2017). We used an approach by Aranovich (2017) to calculate the salt (namely, KCl) concentration in the fluid via reaction

$$Alm + 3Qz + 2KCl = Cl{-}Ann + Kfs \quad (3)$$

(where Cl-Ann is $KFe_3AlSi_3O_{10}Cl_2$ end-member), using standard properties of the KCl melt as properties of this component in the fluid, end-member mineral thermodynamic properties according to Berman (1988) and a solid solution model for garnet from Berman and Aranovich (1996). Using the model by Aranovich and Newton (1997), the obtained value $a_{KCl} = 0.25$ roughly corresponds to $X_{KCl} = 0.32$ and $X_{H2O} = 0.68$ in the CO_2-free aqueous-salt fluid. Water activity in the fluid is about 0.46. Cl-rich biotite is observed exclusively in the assemblage with late garnet(+sillimanite + quartz) forming in the metapelitic enclaves in granites at temperatures below 750 °C, further testifying to the late interaction of the aqueous-salt fluid with the metapelite remnants.

9.2. Mechanism of graphite formation

As discussed above, the relation $\delta^{13}C^{Gr}_{PDB} < \delta^{13}C^{fluid}_{PDB}$ for the studied samples (Table 3) is consistent with the case of near-equilibrium fractionation between graphite and CO_2 fluid (Bottinga, 1969; Friedman and O'Neil, 1977; Scheele and Hoefs, 1992; Polyakov and Kharlashina, 1995), suggesting that they are genetically linked and that formation of graphite is directly related to the evolution of the CO_2-rich fluid phase of the granitic magma. We assume that graphite in granitoids crystallized due to reduction of CO_2 during interaction of the metapelite material with the magma. In this scenario, the plausible factor, which led to the graphite precipitation, was oxidation reactions with participation of sulfides, and in particular pyrrhotite:

$$4Po + CO_2 = 2Py + Gr + 2[FeO], \quad (4)$$

where FeO is a component of silicates (for example, garnet). Reaction (4) is the reverse reaction proposed by various authors (Ferry, 1981; Mohr and Newton, 1983; Hall, 1986; Tracy and Robinson, 1988) to explain transformation of pyrite to pyrrhotite in regionally metamorphosed graphite-bearing pelitic rocks. Abundance of pyrrhotite in host metapelites and its shift to pyrite in granitoids (Table 1; Fig. 5*f*) supports the conclusions. The reaction (4) could operate in the granitoid melts and supply additional FeO to the crystalline phases and melts. However, pyrite is not stable above ~860 °C at 8–8.5 kbar, being decomposed to FeS + S_2 (liquid) (e.g. Kullerud and Yoder, 1959; Barker and Parks, 1986). At temperatures of the granitoid magma (above 900 °C), sulfur could be dissolved in the Fe-poor silicate melt via the following mechanism (e.g. Poulson and Ohmoto, 1990)

$$Po + O^{2-}\ (melt) = FeO\ (melt) + S^{2-}\ (melt), \quad (5)$$

again providing additional FeO to the melt. Pyrite formed later on cooling.

Many authors (Ferry, 1981; Mohr and Newton, 1983; Hall, 1986; Tracy and Robinson, 1988) provide evidence for regular changes in

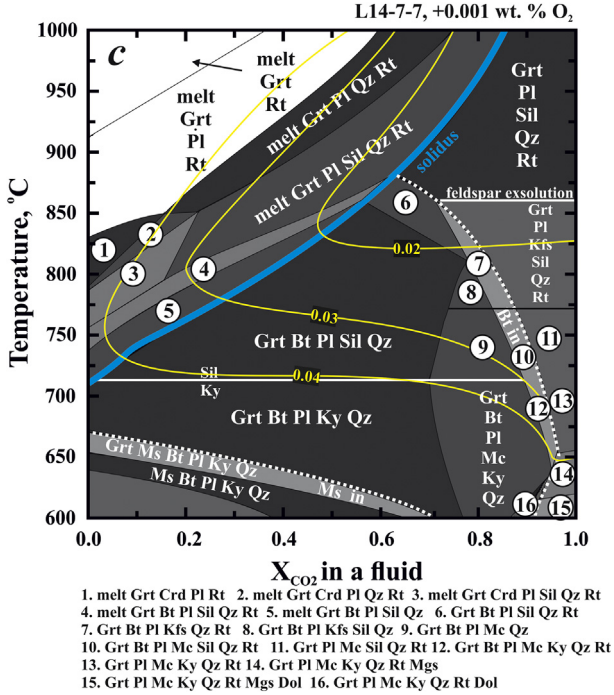

Mg-numbers of silicates coexisting with sulfides, so that Fe-richer silicates coexist with pyrite in contrast to silicates coexisting with pyrrhotite. This regularity seems to be also applied to granitoids of the Bandelierkop quarry. Fig. 6 clearly shows that garnets from the granitoids show a tendency to have lower X_{Mg} in comparison to relic garnets from the biotite-garnet-cordierite enclaves and metapelites. Especially, this feature is important for garnets dispersed in the quartz-feldspathic matrix. In contrast to the garnet from the enclaves, garnets in the quartz-feldspathic matrix isolated from the enclaves had no possibility for active Mg-Fe exchange during cooling and, thus, preserved their initial X_{Mg}.

Appearance of graphite at the biotite-garnet and biotite-cordierite-garnet metapelite enclaves in the granitoids (Fig. 5*d*) serves as structural evidence for formation of graphite during interaction of granitic magma with metapelitic material. Compositional similarities of garnet cores from the enclaves and some garnets in granitoids with garnet compositions in garnet-cordierite-biotite metapelites (Fig. 6) suggest that this type of rocks served as a reactant with the fluid-bearing magma. In this case, reaction (4) can be extended to more complex reactions involving both metapelite and granitic phases, for example

$$\mathrm{Po} + 1/8\mathrm{Fe{-}Crd} + 1/8\mathrm{Qz} + 1/4\mathrm{CO_2} = 1/4\mathrm{Alm} + 1/2\mathrm{Py} + 1/4\mathrm{Gr} \quad (6a)$$

$$\mathrm{Po} + 1/5\mathrm{Fe{-}Crd} + 1/4\mathrm{CO_2} = 3/10\mathrm{Alm} + 1/2\mathrm{Py} + 1/4\mathrm{Gr} + 1/10\mathrm{Sil} \quad (6b)$$

These reactions are displaced to the right with increasing CO_2 activity. The predominant role of CO_2 in the fluid, which accompanied magmas during their intrusion into metapelites, has been discussed in the previous section.

Fluids issued from the granitoids should be able to penetrate host metapelites and provoke the same reactions. In fact, examination of various metapelites contacting to granitoid bodies revealed the presence of rare graphite. Graphite associated with plagioclase developed between orthopyroxene and garnet grains (Fig. 15*a*) in semipelites indicates precipitation during or after the decompression event that is expressed by the reaction Grt + Qz = Opx + Pl. In metapelites, graphite forms with the products of the decompression reaction Grt + Qz = Opx + Crd, as well as with biotite + sillimanite + quartz assemblages. Locally, graphite is associated with Ca-Mg-Fe carbonates in these textures (Fig. 15*a*). At the same time, primary pyrrhotite is replaced by pyrite, which also is accompanied by carbonates (Fig. 15*b*) reflecting the reaction

$$4\mathrm{Po} + 3\mathrm{CO_2} = 2\mathrm{Py} + \mathrm{Gr} + 2\mathrm{Sd}, \quad (7)$$

Association of graphite with biotite and carbonates suggests its contemporary formation with the late hydration event caused by aqueous-carbonic fluids. Stevens (1997) paid attention to the association of graphite with late orthoamphibole + sillimanite (kyanite) assemblages, as well as with late garnet after cordierite and orthopyroxene in hydrated metapelites of the SMZ at or south of the orthoamphibole-in isograd. He interpreted the formation of graphite as a result of re-deposition of precursor carbon by aqueous fluids issued by granitic magmas. However, similarity of reactions resulting in the graphite precipitation in the granitoids and surrounding rocks suggests that they proceeded in both cases under the influence of similar CO_2-rich fluid. Unfortunately, all attempts to separate small fraction of graphite to measure carbon isotope composition were unsuccessful. Nevertheless, $\delta^{13}C_{PDB} = -5.04‰$ measured for the fluid extracted from thin leucocratic veins in metapelite SA-4-5 (Table 3) suggests that metapelites interacted with fluids, which are similar to those carried by the granitoids.

9.3. Possible sources of carbon in the granitoids

Graphite is rather a common mineral in metapelites of the SMZ of the Limpopo Complex (Vennemann and Smith, 1992; Stevens, 1997; van den Berg and Huizenga, 2001; Huizenga et al., 2014). Following to the textural association of graphite with the products of the late hydration reactions, Stevens (1997) assumed a re-deposition of primary pre-metamorphic carbon in metapelites by essentially H_2O-rich fluids assumed to be issued by crystallizing granitic leucosomes without addition of external carbon during the retrograde hydration event, which took place along the sub-isobaric cooling P-T path. This conclusion was majorly based on the data by Vennemann and Smith (1992), who found that $\delta^{13}C_{PDB}$ values of interstitial graphite in metapelites of both the granulite sub-zone and in the amphibolite sub-zone (south of the orthoamphibole-in isograd in the SMZ) varied from −12.5 to −15.2‰, suggesting a contribution of a reduced organic carbon source (e.g. Valley, 1986). In addition, Vennemann and Smith (1992) observed significant carbon isotope heterogeneity within a single locality (Fig. 1*a*), which include both metapelites (samples P5D, P-A and P-B in Vennemann and Smith, 1992) and leucocratic coarse-grained undeformed pegmatoid garnet-bearing trondhjemite (sample V6D in Vennemann and Smith, 1992). The $\delta^{13}C_{PDB}$ values for graphite in metapelites from this locality vary from −15.0‰ for sample P5D to −9.1 and −9.6‰ for samples P-A and P-B, respectively, collected close to the sample P5D. Following to these authors (Vennemann and Smith, 1992; Stevens, 1997), such small-scale isotopic heterogeneity for graphite argues against a pervasive infiltration of external CO_2 in the SMZ, as have been suggested previously by van Reenen and Hollister (1988).

Vennemann and Smith (1992) also obtained isotopic compositions for graphite from the garnet-bearing trondhjemite sampled close (~5 m) to the above metapelites. In contrast to metapelites, this graphite was found to be much "heavier", $\delta^{13}C_{PDB} = -6.4‰$ (Table 3). Following to the O-isotope data, Vennemann and Smith (1992) concluded that trondhjemites were out of isotopic equilibrium with the adjacent pelitic rocks and suggested their "composite origin from melts being derived from several compositionally different but finely interlayered metasediments". It is clear that mixing of the $\delta^{13}C_{PDB}$ values between samples P5D and V6D would readily produce values for graphite from metapelites P-A and P-B at 32–37% of "the metapelite graphite" with $\delta^{13}C_{PDB} = -15‰$ and, respectively, 68–63% of "the trondhjemite

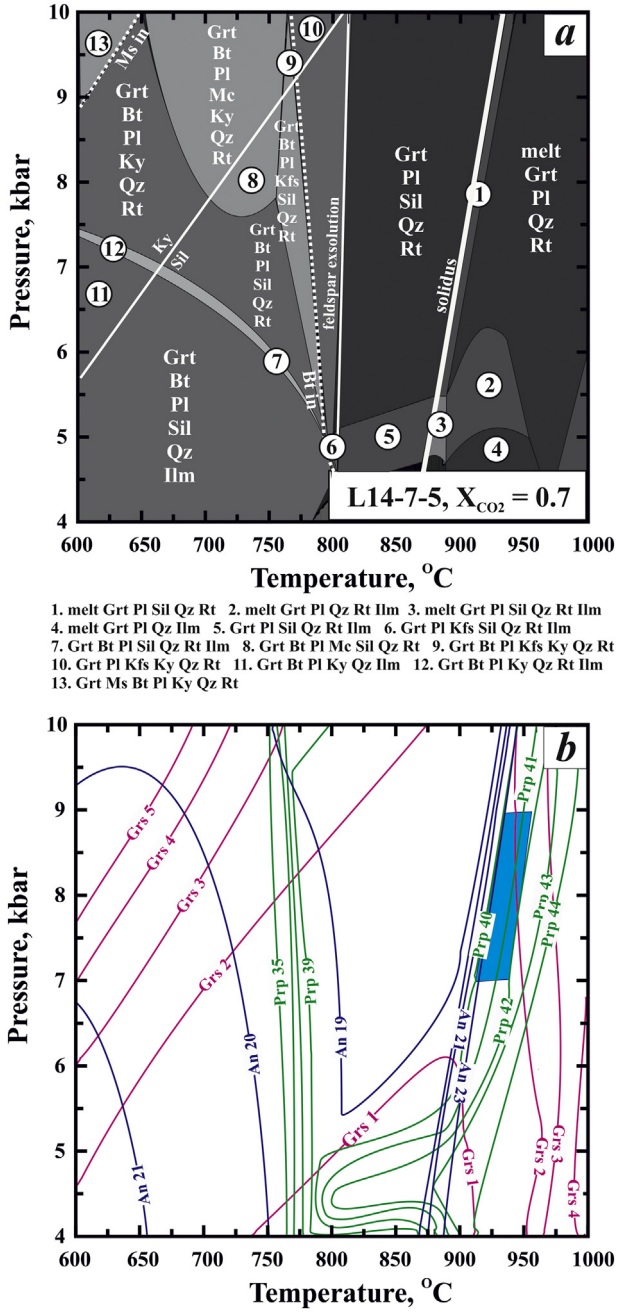

Fig. 13. P-T pseudosection computed for bulk compositions of the sample L14-7-5 (*a*) and selected isopleths of pyrope (green lines Prp 35–Prp 44) and grossular (magenta lines Grs 1–Grs 5) contents of garnet, and anorthite content (dark-blue lines An 19–An 21) of plagioclase (*b*). The light-blue field marks the convergence of the mineral compositions observed in the sample L14-7-5. (For interpretation of the references to color in this figure legend, the reader is referred to the web version of this article.)

graphite" with $\delta^{13}C_{PDB} = -6.4‰$. Such mixing can be mediated by a fluid, which would have heavier $\delta^{13}C_{PDB}$ values in equilibrium with graphite (Bottinga, 1969; Friedman and O'Neil, 1977; Scheele and Hoefs, 1992; Polyakov and Kharlashina, 1995). Similar isotopic mixing of pre-existing isotopically light ($\delta^{13}C_{PDB} = -19.3‰$) carbon with heavier carbon ($\delta^{13}C_{PDB} = -8.1‰$) precipitated from CO_2-rich fluid issued by granitic magmas has been proposed by Farquhar and Chacko (1991) to explain regular variations of $\delta^{13}C_{PDB}$ in graphite along traverses in host rocks around a charnockite dyke at Ponmudi, Southern India.

The situation regarding granitoids of the Bandelierkop quarry seems to be similar to that described by Vennemann and Smith (1992). From correlation of $\delta^{18}O$ with the composition of trondhjemite from the Banderlierkop quarry, Dubinina et al. (2015) also concluded that granitoids were beyond the complete isotopic equilibration with the surrounding rocks, suggesting their source unrelated to the host metapelite. Graphite from the Bandelierkop granitoids is isotopically similar (Table 2) to graphite from garnet-bearing pegmatite veins described by Vennemann and Smith (1992). These data indicate that the magmas forming the garnet granitoids in the SMZ carried carbon-bearing fluids, the source of which is unrelated to pre-metamorphic carbon in surrounding metapelites.

Carbon isotope compositions of graphite from the granitoids associated with the Bandelierkop metapelites (Table 3) lie in the range, which is typical for deep-seated (mantle) carbon sources, i.e. $-6 \pm 2‰$ PDB (e.g. Javoy et al., 1986; Kyser, 1986). "Mantle" $\delta^{13}C$ values for veined graphite in high-grade rocks (e.g. Santosh and Wada, 1993; Santosh and Omori, 2008) and graphite in granitoids accompanying granulites (Farquhar and Chacko, 1991; Satish-Kumar et al., 2011) provided a reason to consider the massive transport of deep-seated CO_2 either through tectonic pathways or via granitic magmas. A similar conclusion also seems to be valid for the SMZ of the Limpopo Complex. van Schalkwyk and van Reenen (1992) and van Reenen et al. (1994) reported $\delta^{13}C = -5.5$ to $-6.0‰$ of CO_2 extracted from magnesite from the retrogressed ultrabasic granulites of the Bandelierkop formation and proposed a deep-seated (possibly mantle) source for the CO_2.

However, different authors (Van Reenen and Hollister, 1988; van Reenen et al., 2014; Kramers et al., 2014) proposed that the fluids that infiltrated hot overlying granulites were produced from devolatilization of the greenstone lithologies of the Kaapvaal craton that underlies >60% of the SMZ in the footwall of the shallow north-dipping HRSZ (De Beer and Stettler, 1992; van Reenen et al., 2014). The abundance of CO_2 fluid in the granitoids would imply a carbonate-bearing source for the silicic magmas (e.g. Holloway, 1976; Lowenstern, 2001). These could be carbonates associated with lithologies in the greenstone belts adjacent to the SMZ (Fig. 1). Groves et al. (1988) recognized two carbon sources in greenstone belts of Western Australia that predate regional metamorphism: sea-floor carbonate alteration characterized by $\delta^{13}C_{PDB} = -2$ to $-3‰$ and fault-controlled regional alteration characterized by $\delta^{13}C_{PDB} = -4$ to $-6‰$. Powell et al. (1991) generalized that "heavy" ($\delta^{13}C = -3$ to $-5‰$) carbon source was specific characteristic for metamorphism of Archean greenstone rocks. Many publications on various Archean greenstone belts (e.g. Burrows et al., 1986; Kerrich et al., 1987; Kerrich, 1989, 1990; Sarangi et al., 2012) indicate that the source with $\delta^{13}C_{PDB} = -0.5$ to $-9‰$ was, apparently, linked to hydrothermal carbonate veins (including ones associated with lode gold deposits) presumably formed by the influx of CO_2-rich fluids. The origin of these fluids is generally uncertain, but a mantle contribution cannot be ruled out (e.g. Kerrich et al., 1987). We are not aware published carbon isotope data on carbonate-bearing rocks of the Gyani, Rhenosterkoppies and Pietersburg greenstone belts immediately adjacent to the SMZ (Fig. 1*a*). However, such data are available for hydrothermal carbonates of the Barberton greenstone belt (De Ronde et al., 1992; Schürmann et al., 2000) that indicates $\delta^{13}C_{PDB}$ values in the range -2.2 to $-4.9‰$. Heavy $\delta^{13}C_{PDB}$ (-1.2 to $-5.8‰$) values are also known for hydrothermal carbonates in the tonalite-trondhjemite-granodiorite Kaap Valley batholith in the Barberton Mountain Land that overlap with the $\delta^{13}C_{PDB}$ values for greenstone lithologies of this greenstone belt (Faure and Harris, 1991). These data can surely be extended to include the worldwide database (see references in the Table 1 in Sarangi et al., 2012), which covers the whole range of the $\delta^{13}C_{PDB}$ values measured for both graphite and fluid inclusions from the granitoids of the Bandelierkop formation (Fig. 16).

10. Conclusion

Discordant contacts (Fig. 2*a–c*) and slight internal foliation of granitoid bodies imply that tonalites, trondhjemites and granites of the

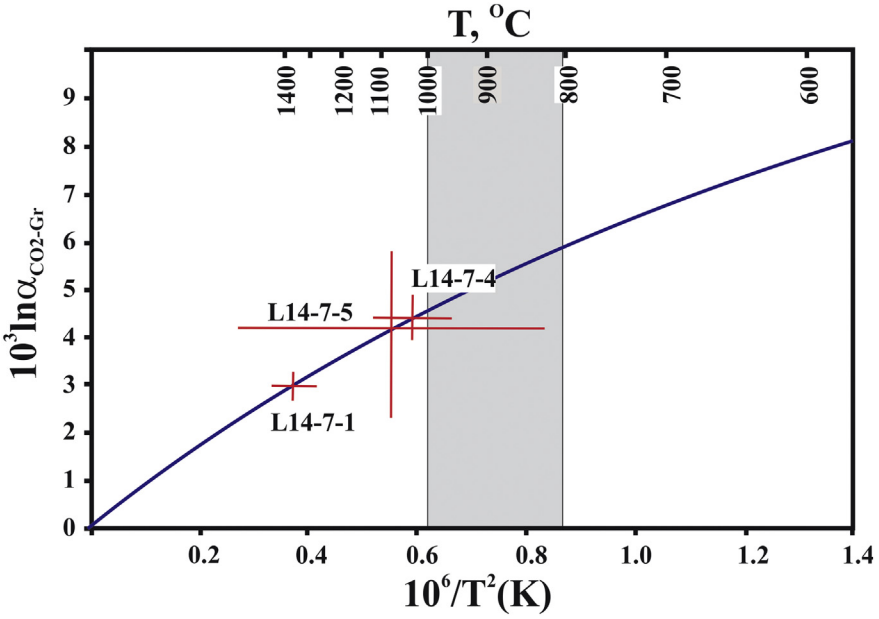

Fig. 14. Isotope fractionation between graphite and carbonic fluids from fluid inclusions in the Bandelierkop granitoids. The equilibrium fractionation curve is shown according to Polyakov and Kharlashina (1995). Grey field indicates a temperature interval estimated from re-integrated ternary feldspars (Fig. 7).

Bandelierkop quarry were emplaced syn- to post-tectonically with respect to the regional shear deformational events that occurred at ~2.72–2.69 Ga after peak metamorphism (Kreissig et al., 2001; Smit et al., 2014; van Reenen et al., 2014). Temperature values above 900 °C obtained for these rocks agree with temperatures obtained for a similar trondhjemite body, which intruded and assimilated metapelites at the Petronella locality, which is located about 20 km to the south-west (Safonov et al., 2014; G.A. Belyanin et al., 2014; G. Belyanin et al., 2014). Thus, tonalites, trondhjemites and granites of the Bandelierkop quarry are, probably, hybrid rocks crystallized from tonalite-trondhjemite magmas variously contaminated by the host metapelites (Safonov et al., 2014). Garnet, sillimanite, rutile and spinel in these rocks were formed during either the assimilation process or caught from the host metapelites. Graphite in the granitoids was produced from the fluid modification in the course of the magma intrusion into granulites. Reduction of CO_2 to graphite occurred both during interaction of the fluids with country granulites and as a result of magma contamination by reduced sulfide-bearing metapelite material.

Carbon isotope data on graphite and fluid inclusions (Table 3) provides conclusive evidence that high-temperature granitoid magmas that crystallized as tonalites and trondhjemites carried CO_2-dominated fluids that originated from a source unrelated to the host metapelites and semi-pelites of the Bandelierkop Formation. These data do not only indicate an external source for the fluids, but also suggest that source for the granitoids was not related to metapelitic granulites, as well (Safonov et al., 2014; van Reenen et al., 2014; Dubinina et al., 2015). The variability of $\delta^{13}C_{PDB}$ between −2.50 and −8.65‰ (Table 3) is also much more consistent with a heterogeneous source for carbon, rather than a homogeneous mantle source. The compilation of published isotopic data (Fig. 16) suggests that carbonate-bearing greenschists or amphibolites from the adjacent greenstone belts on the Kaapvaal Craton are a more reasonable source. High contents of Al_2O_3, CaO and Na_2O combined with the low K_2O content of the granitoids (Fig. 3*a*–*c*) also suggests a metabasaltic or amphibolitic source (Beard and Lofgren, 1991; Rapp et al., 1991; Rushmer, 1991; Wolf and Wyllie, 1994; Patiño Douce and Beard, 1995; Skjerlie and Patino Douce, 1995; Sisson et al., 2005; Moyen and Stevens, 2006; Clemens et al., 2006). Experimental studies (see review in Moyen and Stevens, 2006) show that melting of amphibolites is able to produce tonalite-trondhjemite-granodiorite melts within a wide pressure range of temperatures between 900 and 1000 °C consistent with our thermodynamic modeling (Fig. 12*a*, *b*). This implies a close relationship of these magmas with commencement of interaction of the overriding SMZ granulite with underthrusted rocks of the greenstone belts of the Northern Kaapvaal Craton at 2720–2690 Ma (e.g. van Reenen and Hollister, 1988; van Reenen et al., 2011, 2014; Kramers et al., 2014). Whether underthrusted amphibolite material from adjacent greenstone belts on the craton might be a possible source, or whether mafic granulites and amphibolites of the SMZ is a more viable source, is matter for future geochemical and isotopic studies.

Acknowledgments

We thank two anonymous reviewers for their constructive suggestions. Fruitful discussions with Veniamin Polyakov (IEM RAS), Leonid Aranovich and Elena Dubinina (IGEM RAS) significantly influenced the paper. We thank Christian Reinke (SPECTRAU, University of Johannesburg) for his assistance with bulk analyses of the samples. We thank Tatiana Dokina (IEM RAS) for X-ray measurements of graphite. The analytical work is supported by the Developing Program of the Moscow State University. The stable isotope study was performed as a part of the project #0330-2016-0013 in the Center for Multi-Elemental and Isotope Research at the Sobolev Institute of Geology and Mineralogy, Siberian Branch RAS, Novosibirsk. The study is fulfilled under the Research Program AAAA-A18-118020590148-3 of the Korzhinskii Institute of Experimental Mineralogy RAS. This research is supported by the Russian Science Foundation (project 18-17-00206 to OGS) (in a part of the study of granulite evolution models) and, partially, by the Russian Foundation for Basic Research (project 16-05-00266 to OGS) (in a part of a study of the fluid-rock interaction). DDvR and ACS thank the National Science Foundation of South Africa (project GUN: 81040).

Appendix A. Analytical procedures

A.1. Bulk-rock analysis

For bulk chemistry analysis, granitoid samples were crushed to a fine powder using a jaw crusher and tungsten carbide swing mill. Glass disks were prepared for XRF analysis as a mixture of 5.9 g of high-purity fused anhydrous flux ($Li_2B_4O_7$ + $LiBO_2$ + LiBr), 0.7 g of the rock powder

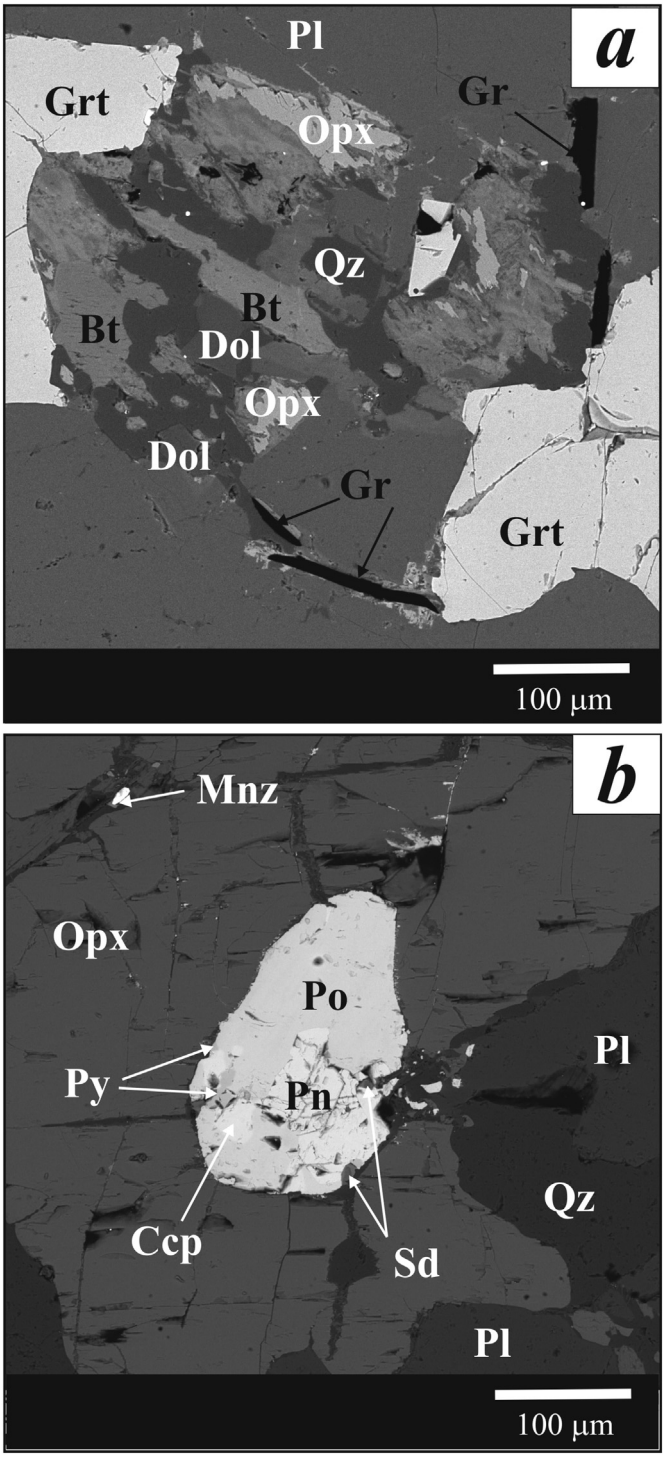

Fig. 15. Reaction textures indicating interaction with the CO_2-rich fluid in metapelites surrounding the granitoid body. (*a*) Graphite and Fe-bearing dolomite associated with the products of garnet decomposition. (*b*) Inclusion of pyrrhotite (+pentlandite + chalcopyrite) in orthopyroxene partially replaced by pyrite and siderite.

(preliminary dried at 105 °C) and 0.5 g of $LiNO_3$. Whole-rock major element compositions were determined using PANalytical Axios Fast 1 MagiX PRO X-Ray Fluorescent Spectrometer equipped with robotic sample changer at Spectrum (The Central Analytical Facility of the Faculty of Science, University of Johannesburg). For standards of known composition, typical deviation from the reference value is <1% for major elements present at a concentration of >1 wt%. LOI was not measured. Measurements below 0.05 wt% were considered to be zero.

A.2. Microprobe analyses

Microprobe analyses of minerals were performed using CamScan MV2300 (VEGA TS 5130MM) electron microscope equipped with EDS INCA Energy 350 and Tescan VEGA-II XMU microscope equipped with EDS INCA Energy 450 and WDS Oxford INCA Wave 700 at the Institute of Experimental Mineralogy, Chernogolovka, Russia. Analyses were performed at 20 kV accelerating voltage with a beam current up to 400 pA, spot size 115–150 nm and a zone of "excitation" with 3–4 μm diameter. Counting times was 100 s for all elements. The ZAF matrix correction was applied. The following standards were used: SiO_2 for Si and O, albite for Na, microcline for K, wollastonite for Ca, pure titanium for Ti, corundum for Al, pure manganese for Mn, pure iron for Fe, periclase for Mg, BaF_2 for Ba.

The Jeol Superprobe JXA-8230 at the Laboratory of Local Methods of Analysis at the Department of Petrology of the Moscow State University was used to specifically analyze both major and minor elements (Ti, Sc, Y, P, Cr) in garnets. The analytical conditions for the Superprobe analyses were 20 kV acceleration voltage and 60 nA beam current. The slit size was 500 μm for all spectrometers. The garnet standards USNM 143968 (Mg-Kα_1, Al-Kα_1 and Si-Kα_1 – TAP crystal; Fe-Kα_1 – LiF crystal) и USNM 87375 (Ca-Kα_1 – PET-J crystal) were used for calibration of the major elements (Jarosewich et al., 1980). Counting times for major elements were similar both for the standards and the sample: Mg, Ca and Fe – 40 s.; Al and Si – 20 s. The dispersion of the measured concentration during the major element analyses using the above conditions did not exceed 0.5%. The following crystalline standards were used for the minor element analyses: $MnTiO_3$ for Ti-Kα_1 and Mn-Kα_1; Cr_2O_3 for Cr-Kα_1; $ScPO_4$ for P-Kα_1 and Sc-Kα_1; $Y_3Al_5O_{12}$ for Y-Lα_1. The Ti, Mn, Cr measurements (crystal LiF) and P (crystal PET-J) were performed using spectrometers with a 140 mm radius Rowland circle, whereas Sc and Y (crystal PET-H) were measured using the 100 mm radius H-type spectrometer. The position of maxima for the trace elements in garnets was specified by means of slow scanning of the corresponding spectral intervals. Counting time was set to attain the detection limit of 0.005 wt%: 30 s. for Ti and Mn, 40 s. for Cr, 60 s for P and Y and 80 s for Sc. ZAF correction was applied for analyses. Analytical conditions for the elemental mapping at the Jeol Superprobe JXA-8230 were the same as for individual spot analyses. Elemental maps were constructed on the basis of 10 scans with a resolution of 256 × 192 pixels and dwell time 10 ms. All mineral analyses used in this study (see below) are presented in tables collected in the Supplementary materials.

A.3. X-ray diffraction

X-ray diffraction pattern of graphite was obtained using Bruker Advance D8 diffractometer (at the Institute of Experimental Mineralogy) with Cu Kα radiation and Si as internal standard. At these analytical conditions, the interplanar spacing (d_{002}) was determined and c_0 parameter of graphite was calculated.

A.4. Fluid inclusion analysis

Fluid inclusions were investigated in double-polished sections (200 to 300 μm thick) using the LINKAM THMSG 600 heating-freezing stage at the Institute of Experimental Mineralogy. The stage works within the temperature range from −196 °C to 600 °C with automatic heating/cooling at a rate of 0.1–90 °C/min. Accuracy of the thermometric measurements is about ±0.1 °C. Systematic calibration of the stage was performed using natural (CO_2, Camperio, Alps) and synthetic (H_2O) inclusions in quartz.

Qualitative identification of gaseous species in fluid inclusions in quartz and garnet was performed by means of Raman spectroscopy using the JY Horiba XPloRa Jobin spectrometer equipped with a polarized Olympus BX41 microscope at Department of Petrology, Moscow State University, Moscow, Russia. Spectra were obtained using a 532-

nm laser within the range 100–4000 cm^{-1} during 30 s. To better resolve band of volatile species, additional spectra were collected within the range 1200–1300 cm^{-1} with longer exposition time. The spectra were refined with LabSpec (version 5.78.24) software. Assignment of the Raman bands was carried out using a compilation by Frezzotti et al. (2012).

A.5. Carbon isotope analysis

Reutsky et al. (2012) provide details of the procedure and technique for the carbon isotope analysis applied in the present study. In order to measure carbon isotope composition of graphite, 1 mg fractions of the mineral were separated from fresh cleavages of three samples of garnet- and sillimanite-bearing granitoids. The fractions were packed into platinum foil, placed into a reactor tube made of a fused quartz together with a purified CuO and oxidized. The reactor was evacuated to the pressure of 10^{-4} Pa and then heated up to 900 °C for 20 min. Resulting carbon dioxide was purified and transferred to a detachable glass vial. In order to extract CO_2 from the fluid inclusions for the isotope analysis, the rocks were crushed to the fraction 0.5–0.25 mm, and quartz was separated without using any solvents or heavy liquids. Gases adsorbed on the surface of the quartz grains were removed by means of heating of the quartz charge in the vacuumed tube made of a fused quartz at 150 °C and pressure not $>1.5 \cdot 10^{-3}$ mbar. After that, the reactor was sealed and heated up to temperature 800 °C. The α-β transition in quartz provided a complete decrepitation of fluid inclusions. The extracted CO_2 was purified using low-temperature rectification. The carbon isotope composition of CO_2 produced from graphite oxidation and extracted from fluid inclusions were performed using the Finnigan MAT Delta instrument in a dual inlet mode at the Institute of Geology and Mineralogy, Siberian Branch of RAS, Novosibirsk. Variations of $\delta^{13}C$ for individual samples was +0.02–+1.2‰. The USGS-24 standard (graphite with $\delta^{13}C_{PDB} = -15.9‰$) was used to control the isotope analysis procedure. All the $\delta^{13}C_{PDB}$ values are given relative to the PDB standard.

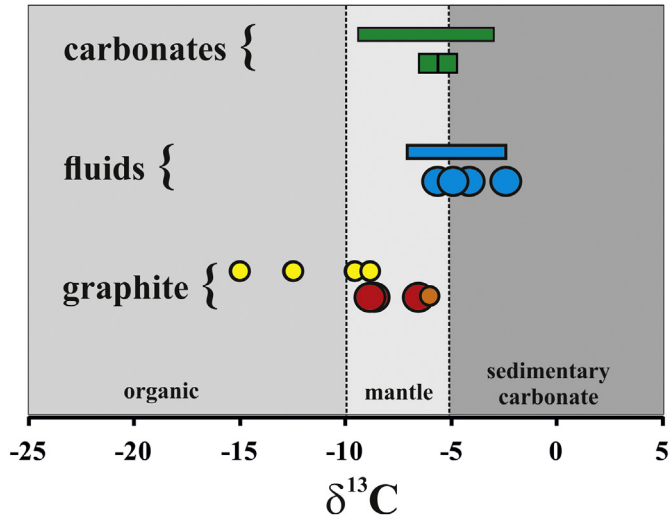

Fig. 16. Compilation of the carbon isotope data on graphite (red circles) and from fluid inclusions (light-blue circles) from the Bandelierkop rocks (Table 3). The data are compared with the following published data on carbon isotope composition: yellow dots - $\delta^{13}C_{PDB}$ for graphite from metapelite of the Bandelierkop Formation (Vennemann and Smith, 1992), orange dot - $\delta^{13}C_{PDB}$ for graphite from a garnet trondhjemite vein (Vennemann and Smith, 1992), green squares - $\delta^{13}C_{PDB}$ for carbonates from meta-ultrabasic granulites of the Bandelierkop Formation (van Schalkwyk and van Reenen, 1992; van Reenen et al., 1994), long green rectangle shows a range of $\delta^{13}C_{PDB}$ for hydrothermal carbonates from greenstone belts (Burrows et al., 1986; Kerrich et al., 1987; Kerrich, 1989, 1990; Sarangi et al., 2012), long light-blue rectangle shows a range of $\delta^{13}C_{PDB}$ for fluid inclusions in quartz and carbonates of hydrothermal veins in greenstone belts (e.g. Sarangi et al., 2012). (For interpretation of the references to color in this figure legend, the reader is referred to the web version of this article.)

Appendix B. Supplementary data

Supplementary data to this article can be found online at https://doi.org/10.1016/j.gr.2018.04.009.

References

Aranovich, L.Y., 2017. The role of brines in high-temperature metamorphism and granitization. Petrology 2, 486–497.

Aranovich, L.Y., Newton, R.C., 1997. H_2O activity in concentrated KCl and KCl-NaCl solutions at high temperatures and pressures measured by the brucite-periclase equilibrium. Contributions to Mineralogy and Petrology 127, 261–271.

Aranovich, L.Y., Safonov, O.G., 2018. Halogens in high-grade metamorphism. In: Harlov, D. E., Aranovich, L.Y. (Eds.), The Role of Halogens in Terrestrial and Extraterrestrial Geochemical Processes, pp. 713–757 (Chapter 11, Springer Geochemistry).

Baker, J., van Reenen, D.D., Van Schalkwyk, J.F., Newton, R.C., 1992. Constraints on the composition of fluids involved in retrograde anthophyllite formation in the Limpopo Belt, South Africa. Precambrian Research 55, 327–336.

Barker, W.W., Parks, T.C., 1986. The thermodynamic properties of pyrrhotite and pyrite: a re-evaluation. Geochimica et Cosmochimica Acta 50, 2185–2194.

Barton, J.M., Van Reenen, D.D., 1992. When was the Limpopo orogeny? Precambrian Research 55, 7–16.

Barton, J.M., Doig, R., Smith, C.B., Bohlender, F., van Reenen, D.D., 1992. Isotopic and REE characteristics of the intrusive charnoenderbite and enderbite geographically associated with the Matok Pluton, Limpopo belt, southern Africa. Precambrian Research 55, 451–567.

Beard, J.S., Lofgren, G.E., 1991. Dehydration melting and water-saturated melting of basaltic and andesitic greenstones and amphibolites at 1, 3, and 6.9 kb. Journal of Petrology 32, 365–401.

Belyanin, G.A., Rajesh, H.M., Van Reenen, D.D., Mouri, H., 2010. Corundum + orthopyroxene ± spinel intergrowths in an ultrahigh-temperature Al-Mg granulite from the Southern Marginal Zone, Limpopo Belt, South Africa. American Mineralogist 95, 196–199.

Belyanin, G.A., Rajesh, H.M., Sajeev, K., van Reenen, D.D., 2012. Ultrahigh-temperature metamorphism from an unusual corundum+orthopyroxene intergrowth bearing Al–Mg granulite from the Southern Marginal Zone, Limpopo Complex, South Africa. Contributions to Mineralogy and Petrology 164, 457–475.

Belyanin, G.A., Kramers, J.D., Vorster, C., Knoper, M.W., 2014. The timing of successive fluid events in the Southern Marginal Zone of the Limpopo Complex, South Africa: constraints from ^{40}Ar–^{39}Ar geochronology. Precambrian Research 254, 169–193.

Belyanin, G., van Reenen, D.D., Safonov, O.G., 2014. Response to comments by Nicoli et al. on the paper by Belyanin et al. (2012). Contributions to Mineralogy and Petrology 167, 1–5.

Berman, R.G., 1988. Internally-consistent thermodynamic data for stoichiometric minerals in the system Na_2O-K_2O-CaO-MgO-FeO-Fe_2O_3-Al_2O_3-SiO_2-TiO_2-H_2O-CO_2. Journal of Petrology 29, 445–522.

Berman, R.G., 2007. WinTWQ (version 2.3): a software package for performing internally-consistent thermobarometric calculations. Geological Survey of Canada Open File 5462.

Berman, R.G., Aranovich, L.Ya, 1996. Optimized standard state and solution properties of minerals I model calibration for olivine, orthopyroxene, cordierite, garnet, and ilmenite in the system FeO-MgO-CaO-Al_2O_3-TiO_2-SiO_2. Contributions to Mineralogy and Petrology 126, 1–24.

Beyssac, O., Goffé, B., Chopin, C., Rouzaud, J.N., 2002. Raman spectra of carbonaceous material in metasediments: a new geothermometer. Journal of Metamorphic Geology 20, 859–871.

Blenkinsop, T.G., 2011. Archean magmatic granulites, diapirism, and Proterozoic reworking in the Northern Marginal Zone of the Limpopo Belt. Geological Society of America Memoirs 207, 245–267.

Bottinga, Y., 1969. Calculated fractionation factors for carbon and hydrogen isotope exchange in the system calcite-carbon dioxide-graphite-methane-hydrogen-water vapor. Geochimica et Cosmochimica Acta 33, 49–64.

Brandt, S., Klemd, R., Li, Q., Kröner, A., Brandl, G., Fischer, A., Bobek, P., Zhou, T., 2018. Pressure-temperature evolution during two granulite-facies metamorphic events (2.62 and 2.02 Ga) in rocks from the Central Zone of the Limpopo Belt, South Africa. Precambrian Research https://doi.org/10.1016/j.precamres.2018.03.002 (in press).

Burrows, D.R., Wood, P.C., Spooner, E.T.C., 1986. Carbon isotope evidence for a magmatic origin for Archaean gold-quartz vein ore deposits. Nature 321, 851–854.

Cesare, B., Meli, S., Nodari, L., Russo, U., 2005. Fe^{3+} reduction during biotite melting in graphitic metapelites: another origin of CO_2 in granulites. Contributions to Mineralogy and Petrology 149, 129–140.

Clemens, J.D., Yearron, L.M., Stevens, G., 2006. Barberton (South Africa) TTG magmas: geochemical and experimental constraints on source-rock petrology, pressure of formation and tectonic setting. Precambrian Research 151, 53–78.

Clemens, J.D., Stevens, G., Farina, F., 2011. The enigmatic source of I-type granites: the peritectic connexion. Lithos 126, 174–181.

Connolly, J.A.D., 2005. Computation of phase equilibria by linear programming: a tool for geodynamic modeling and its application to subduction zone decarbonation. Earth and Planetary Science Letters 236, 524–541.

De Beer, J.H., Stettler, E.H., 1992. The deep structure of the Limpopo Belt from geophysical studies. Precambrian Research 55, 173–186.

De Ronde, C.E.J., Spooner, E.T.C., de Wit, M.J., Bray, C.J., 1992. Shear zone-related, Au quartz vein deposits in the Barberton greenstone belt, South Africa; field and petrographic characteristics, fluid properties, and light stable isotope geochemistry. Economic Geology 87, 366–402.

van den Berg, R., Huizenga, J., 2001. Fluids in granulites of the Southern Marginal Zone of the Limpopo belt, South Africa. Contributions to Mineralogy and Petrology 141, 529–545.
van den Kerkhof, A.M., Thiéry, R., 2001. Carbonic inclusions. Lithos 55, 49–68.
Du Toit, M.C., Van Reenen, D.D., Roering, C., 1983. Some aspects of the geology, structure and metamorphism of the Southern Marginal Zone of the Limpopo Metamorphic Complex. Special Publication of the Geological Society of South Africa. 8, pp. 121–142.
Dubinina, E.O., Aranovich, L.Y., van Reenen, D.D., Avdeenko, A.S., Varlamov, D.A., Shaposhnikov, V.V., Kurdyukov, E.B., 2015. Involvement of fluids in the metamorphic processes within different zones of the Southern Marginal Zone of the Limpopo complex, South Africa: an oxygen isotope perspective. Precambrian Research 256, 48–61.
Duke, E.F., Rumble, D., 1986. Textural and isotopic variations in graphite from plutonic rocks, south-central New Hampshire. Contributions to Mineralogy and Petrology 93, 409–419.
Elkins, L.T., Grove, T.L., 1990. Ternary feldspar experiments and thermodynamic models. American Mineralogist 75, 544–559.
Farquhar, J., Chacko, T., 1991. Isotopic evidence for involvement of CO_2-bearing magmas in granulite formation. Nature 354, 60–63.
Faure, K., Harris, C., 1991. Oxygen and carbon isotope geochemistry of the 3.2 Ga Kaap Valley tonalite, Barberton greenstone belt, South Africa. Precambrian Research 52, 301–319.
Ferry, J.M., 1981. Petrology of graphitic sulfide-rich schists from south-central Maine: an example of desulfidation during prograde regional metamorphism. American Mineralogist 66, 908–930.
Frezzotti, M.L., Tecce, F., Casagli, A., 2012. Raman spectroscopy for fluid inclusion analysis. Journal of Geochemical Exploration 112, 1–20.
Friedman, I., O'Neil, J.R., 1977. Data of geochemistry. In: Fleisher, M. (Ed.), Compilation of Stable Isotope Fractionation Factors of Geochemical Interest, United States Geological Survey, Professional Paper 440-kk, 6h ed..
Frost, B.R., Frost, C.D., 1987. CO_2, melts and granulite metamorphism. Nature 327, 503–506.
Frost, B.R., Frost, C.D., Touret, J.L., 1989. Magmas as a source of heat and fluids in granulite metamorphism. Fluid Movements—Element Transport and the Composition of the Deep Crust. Springer Netherlands, pp. 1–18.
Fuhrman, M.L., Lindsley, D.H., 1988. Ternary-feldspar modeling and thermometry. American Mineralogist 73, 201–215.
Gardien, V., Thompson, A.B., Ulmer, P., 2000. Melting of biotite + plagioclase + quartz gneisses: the role of H_2O in the stability of amphibole. Journal of Petrology 41, 651–666.
Giorgetti, G., Frezzotti, M.L., Palmeri, R., Burke, E.A.J., 1996. Role of fluids in migmatites: CO_2-H_2O fluid inclusions in leucosomes from the Deep Freeze Range migmatites (Terra Nova Bay, Antarctica). Journal of Metamorphic Geology 14, 307–317.
Glassley, W., 1982. Fluid evolution and graphite genesis in the deep continental crust. Nature 295, 229–231.
Groves, D.I., Golding, S.D., Rock, N.M.S., Barley, M.E., McNaughton, N.J., 1988. Archean carbon reservoirs and their relevance to fluid source for gold deposits. Nature 331, 254–257.
Hall, A.J., 1986. Pyrite-pyrrhotine redox reactions in nature. Mineralogical Magazine 50, 223–229.
Holland, T.J.B., Powell, R., 2011. An improved and extended internally consistent thermodynamic dataset for phases of petrological interest, involving a new equation of state for solids. Journal of Metamorphic Geology 29, 333–383.
Hollister, L.S., 1988. On the origin of CO_2-rich fluid inclusions in migmatites. Journal of Metamorphic Geology 6, 467–474.
Hollister, L.S., 1990. Enrichment of CO_2 in fluid inclusions in quartz by removal of H_2O during crystal-plastic deformation. Journal of Structural Geology 12, 895–901.
Holloway, J.R., 1976. Fluids in evolution of granitic magmas: consequence of finite CO_2 solubility. Geological Society of America Bulletin 87, 1513–1518.
Huizenga, J.M., 2011. Thermodynamic modelling of a cooling C–O–H fluid–graphite system: implications for hydrothermal graphite precipitation. Mineralium Deposita 46, 23–33.
Huizenga, J.M., Touret, J.L., 2012. Granulites, CO_2 and graphite. Gondwana Research 22, 799–809.
Huizenga, J.M., Van Reenen, D., Touret, J.L., 2014. Fluid-rock interaction in retrograde granulites of the Southern Marginal Zone, Limpopo high grade terrain, South Africa. Geoscience Frontiers 5, 673–682.
Jackson, D.H., Mattey, D.P., Harris, N.B.W., 1988. Carbon isotope compositions of fluid inclusions in charnockites from southern India. Nature 333, 167–170.
Jarosewich, E., Nelen, J.A., Norberg, J.A., 1980. Reference samples for electron microprobe analysis. Geostandards Newsletter 4, 43–47.
Javoy, M., Pineau, F., Delorme, H., 1986. Carbon and nitrogen isotopes in the mantle. Chemical Geology 57, 41–62.
Kanaris-Sotiriou, R., 1997. Graphite-bearing peraluminous dacites from the Erlend volcanic complex, Faeroe-Shetland Basin, North Atlantic. Mineralogical Magazine 61, 175–184.
Kerrich, R., 1989. Archean gold: relation to granulite formation or felsic intrusions? Geology 17, 1011–1015.
Kerrich, R., 1990. Carbon-isotope systematics of Archean Au–Ag vein deposits in the Superior Province. Canadian Journal of Earth Sciences 27, 40–56.
Kerrich, R., Fryer, B.J., King, R.W., Willmore, L.M., Hees, E.V., 1987. Crustal outgassing and LILE enrichment in major lithosphere structures, Archean Abitibi greenstone belt: evidence on the source reservoir from strontium and carbon isotope tracers. Contributions to Mineralogy and Petrology 97, 156–168.
Koester, E., Pawley, A.R., Fernandes, L.A.D., Porcher, C.C., Soliani Jr., E., 2002. Experimental melting of cordierite gneiss and the petrogenesis of syntranscurrent peraluminous granites in southern Brazil. Journal of Petrology 39, 689–710.
Koizumi, T., Tsunogae, T., van Reenen, D.D., 2014. Fluid evolution of partially retrogressed pelitic granulite from the Southern Marginal Zone of the Neoarchean Limpopo Complex, South Africa: evidence from phase equilibrium modelling. Precambrian Research 253, 146–156.
Kramers, J.D., Zeh, A., 2011. A review of Sm-Nd and Lu-Hf isotope studies in the Limpopo Complex and adjoining cratonic areas, and their bearing on models of crustal evolution and tectonism. Geological Society of America Memoirs 207, 163–188.
Kramers, J.D., McCourt, S., Roering, C., Smit, C.A., van Reenen, D.D., 2011. Tectonic models proposed for the Limpopo Complex: mutual compatibilities and constraints. Geological Society of America Memoirs 207, 311–324.
Kramers, J.D., Henzen, M., Steidle, L., 2014. Greenstone belts at the northernmost edge of the Kaapvaal Craton: timing of tectonic events and a possible crustal fluid source. Precambrian Research 253, 96–113.
Kreissig, K., Nagler, T.F., Kramers, J.D., Van Reenen, D.D., Smit, C.A., 2000. An isotopic and geochemical study of the northern Kaapvaal Craton and the Southern Marginal Zone of the Limpopo Belt: are they juxtaposed terranes? Lithos 50, 1–25.
Kreissig, K., Holzer, L., Frei, R., 2001. Geochronology of the Hout River Shear Zone and the metamorphism in the Southern Marginal Zone of the Limpopo Belt, southern Africa. Precambrian Research 109, 145–173.
Kröner, A., Brandl, G., Brandt, S., Klemd, R., Xie, H., 2018. Geochronological evidence for Archaean and Palaeoproterozoic polymetamorphism in the Central Zone of the Limpopo Belt, South Africa. Precambrian Research *310*, 320–347.
Kullerud, G., Yoder, H.S., 1959. Pyrite stability relations in the Fe-S system. Economic Geology 54, 533–572.
Kyser, T.K., 1986. Stable isotope variations in the mantle. In: Valley, J.W., Taylor, H.P., O'Niel, J.R. (Eds.), Stable Isotopes in High Temperature Geological Processes. Book-Crafters, Chelsea, MI, pp. 141–164.
Lamb, W.M., Valley, J.W., 1985. COH fluid calculations and granulite genesis. The Deep Proterozoic Crust in the North Atlantic Provinces. Springer Netherlands, pp. 119–131.
Lamb, W.M., Valley, J.W., Brown, P.E., 1987. Post-metamorphic CO_2-rich fluid inclusions in granulites. Contributions to Mineralogy and Petrology 96, 485–495.
Laurent, O., Zeh, A., 2015. A linear Hf isotope-age array despite different granitoid sources and complex Archean geodynamics: example from the Pietersburg block (South Africa). Earth and Planetary Science Letters 430, 326–338.
Laurent, O., Paquette, J.L., Martin, H., Doucelance, R., Moyen, J.F., 2013. LA-ICP-MS dating of zircons from Meso-and Neoarchean granitoids of the Pietersburg block (South Africa): crustal evolution at the northern margin of the Kaapvaal craton. Precambrian Research 230, 209–226.
Laurent, O., Rapopo, M., Stevens, G., Moyen, J.F., Martin, H., Doucelance, R., Bosq, C., 2014. Contrasting petrogenesis of Mg-K and Fe-K granitoids and implications for post-collisional magmatism: case study from the Late-Archean Matok pluton (Pietersburg block, South Africa). Lithos 196-197, 131–149.
Le Breton, N., Thompson, A.B., 1988. Fluid-absent (dehydration) melting of biotite in metapelites in the early stages of crustal anatexis. Contributions to Mineralogy and Petrology 99, 226–237.
Le Maitre, R.W., Streckeisen, A., Zanettin, B., Le Bas, M.J., Bonin, B., Bateman, P., Bellieni, G., Dudek, A., Efremova, S., Keller, J., Lameyre, J., Sabine, P.A., Schmid, R., Sörensen, H., Wooley, A.R., 2002. Igneous rocks – a classification and glossary of terms. Recommendations of the IUGS Subcommission on the Systematics of Igneous Rocks, 2nd edition Cambridge University Press, Cambridge.
Lowenstern, J.B., 2001. Carbon dioxide in magmas and implications for hydrothermal systems. Mineralium Deposita 36, 490–502.
Luque, F.J., Barrenechea, J.F., Rodas, M., 1993. Graphite geothermometry in low and high temperature regimes: two case studies. Geological Magazine 130, 501–511.
Luque, F.J., Crespo-Feo, E., Barrenechea, J.F., Ortega, L., 2012. Carbon isotopes of graphite: implications on fluid history. Geoscience Frontiers 3, 197–207.
McLelland, J., Hunt, W.M., Hansen, E.C., 1988. The relationship between metamorphic charnockite and marble near Speculator, central Adirondack Mountains, New York. Journal of Geology 96, 455–467.
Mohr, D.W., Newton, R.C., 1983. Kyanite-staurolite metamorphism in sulfidic schists of the Anakeesta formation, Great Smoky Mountains, North Carolina. American Journal of Science 283, 97–134.
Moyen, J.-F., Stevens, G., 2006. Experimental constraints on TTG petrogenesis: implications for Archean geodynamics. Geophysical Monograph Series. 164, pp. 149–175.
Munoz, J.L., Swenson, A., 1981. Chloride-hydroxyl exchange in biotite and estimation of relative HC1/HF activities in hydrothermal fluids. Economic Geology 76, 2212–2221.
Newton, R.C., Smith, J.C., Windley, B.F., 1980. Carbonic metamorphism, granulites and crustal growth. Nature 288, 45–50.
Newton, R.C., Touret, J.L., Aranovich, L.Y., 2014. Fluids and H_2O activity at the onset of granulite facies metamorphism. Precambrian Research 253, 17–25.
Ni, H., Keppler, H., 2013. Carbon in silicate melts. Reviews in Mineralogy and Geochemistry 75, 251–287.
Nicoli, G., Stevens, G., Buick, I.S., Moyen, J.-F., 2014. A comment on ultrahigh-temperature metamorphism from an unusual corundum+orthopyroxene intergrowth bearing Al–Mg granulite from the Southern Marginal Zone, Limpopo Complex, South Africa by Belyanin et al. Contributions to Mineralogy and Petrology 167, 1022.
Nicoli, G., Stevens, G., Moyen, J.-F., Frei, D., 2015. Rapid evolution from sediment to anatectic granulite in an Archean continental collision zone: the example of the Bandelierkop Formation metapelites, South Marginal Zone, Limpopo Belt, South Africa. Journal of Metamorphic Geology 33, 177–202.
Pasteris, J.D., 1989. In situ analysis in geological thin-sections by laser Raman microprobe spectroscopy: a cautionary note. Applied Spectroscopy 43, 567–570.
Patino Douce, A.E., 1997. Generation of metaluminous A-type granites by low-pressure melting of calc-alkaline granitoids. Geology 25, 743–746.
Patiño Douce, A.E., Beard, J.S., 1995. Dehydration-melting of biotite gneiss and quartz amphibolite from 3 to 15 kbar. Journal of Petrology 36, 707–738.

Patiño Douce, A.E., Harris, N., 1998. Experimental constraints on Himalayan anatexis. Journal of Petrology 39, 689–710.
Patiño Douce, A.E., Johnston, D.A., 1991. Phase equilibria and melt productivity in the pelitic system: implications for the origin of peraluminous granitoids and aluminous granulites. Contributions to Mineralogy Petrology 107, 202–218.
Perchuk, L.L., Gerya, T.V., van Reenen, D.D., Safonov, O.G., Smit, C.A., 1996. The Limpopo Metamorphic Belt, South Africa: 2. Decompression and cooling regimes of granulites and adjacent rocks of the Kaapvaal Craton. Petrology 4, 571–599.
Perchuk, L.L., Gerya, T.V., van Reenen, D.D., Smit, C.A., Krotov, A.V., Safonov, O.G., 2000. Comparative petrology and metamorphic evolution of the Limpopo (South Africa) and Lapland (Fennoscandia) high grade terrains. Mineralogy and Petrology 69, 69–107.
Perchuk, L.L., Van Reenen, D.D., Varlamov, D.A., Van Kal, S.M., Boshoff, R., 2008. P–T record of two high-grade metamorphic events in the Central Zone of the Limpopo Complex, South Africa. Lithos 103, 70–105.
Pickering, G.M., Johnston, D.A., 1998. Fluid-absent melting behavior of a two-mica metapelite: experimental constraints on the origin of Black Hills granite. Journal of Petrology 39, 1787–1804.
Polyakov, V.B., Kharlashina, N.N., 1995. The use of heat capacity data to calculate carbon isotope fractionation between graphite, diamond, and carbon dioxide: a new approach. Geochimica et Cosmochimica Acta 59, 2561–2572.
Poulson, S.R., Ohmoto, H., 1990. An evaluation of the solubility of sulfide sulfur in silicate melts from experimental data and natural samples. Chemical Geology 85, 57–75.
Powell, R., Will, T.M., Phillips, G.N., 1991. Metamorphism in Archaean greenstone belts: calculated fluid compositions and implications for gold mineralization. Journal of Metamorphic Geology 9, 141–150.
Putnis, A., 2002. Mineral replacement reactions: from macroscopic observations to microscopic mechanisms. Mineralogical Magazine 66, 689–708.
Radhika, U.P., Santosh, M., 1996. Shear-zone hosted graphite in southern Kerala, India: implications for CO_2 infiltration. Journal of Southeast Asian Earth Sciences 14, 265–273.
Rajesh, H.M., Santosh, M., Wan, D., Liu, S., Liu, S.J., Belyanin, G.A., 2014. Ultrahigh temperature granulites and magnesian charnockites: evidence for Neoarchean accretion along the northern margin of the Kaapvaal craton. Precambrian Research 246, 150–159.
Rapp, R.P., Watson, E.B., Miller, C.F., 1991. Partial melting of amphibolite/eclogite and the origin of Archean trondhjemites and tonalites. Precambrian Research 51, 1–25.
van Reenen, D.D., 1983. Cordierite + garnet + hypersthene + biotite-bearing assemblages as a function of changing metamorphic conditions in the Southern Marginal Zone of the Limpopo metamorphic complex, South Africa. Geological Society of South Africa Special Publication 8, 143–167.
van Reenen, D.D., 1986. Hydration of cordierite and hypersthene and a description of the retrograde orthoamphibole isograd in the Limpopo Belt, South Africa. American Mineralogist 71, 900–915.
van Reenen, D.D., Hollister, L.S., 1988. Fluid inclusions in hydrated granulite facies rocks, southern marginal zone of the Limpopo Belt, South Africa. Geochimica et Cosmochimica Acta 52, 1057–1064.
van Reenen, D.D., Barton, J.M., Roering, C., Smit, C.A., van Schalkwyk, J.F., 1987. Deep crustal response to continental collision: the Limpopo belt of southern Africa. Geology 15, 11–14.
van Reenen, D.D., Pretorius, A.I., Roering, C., 1994. Characterization of fluids associated with gold mineralization and with regional high-temperature retrogression of granulites in the Limpopo belt, South Africa. Geochimica et Cosmochimica Acta 58, 1147–1159.
van Reenen, D.D., Smit, C.A., Perchuk, L.L., Roering, C., Boshoff, R., 2011. Thrust exhumation of the Neoarchean ultrahigh-temperature Southern Marginal Zone, Limpopo Complex: convergence of decompression-cooling paths in the hanging wall and prograde P-T paths in the footwall. Geological Society of America Memoirs 207, 189–212.
van Reenen, D.D., Huizenga, J.-M., Smit, C.A., Roering, C., 2014. Fluid-rock interaction during high-grade metamorphism: instructive examples from the Southern Marginal Zone of the Limpopo Complex, South Africa. Precambrian Research 253, 63–80.
Retief, E.A., Compston, W., Armstrong, R.A., Williams, I.S., 1990. Characteristics and preliminary U–Pb ages of zircons from Limpopo Belt lithologies. Extended Abstracts, Limpopo Workshop. Rand Afrikaans University, Johannesburg, South Africa, pp. 95–99.
Reutsky, V.N., Borzdov, Y.M., Palyanov, Y.N., 2012. Effect of diamond growth rate on carbon isotope fractionation in Fe–Ni–C system. Diamond and Related Materials 21, 7–10.
Rodas, M., Luque, F.J., Barrenechea, J.F., Fernández-Caliani, J.C., Miras, A., Fernández-Rodríguez, C., 2000. Graphite occurrences in the low-pressure/high-temperature metamorphic belt of the Sierra de Aracena (southern Iberian Massif). Mineralogical Magazine 64, 801–814.
Roering, C., Van Reenen, D.D., Smit, C.A., 1992. Tectonic model for the evolution of the Limpopo Belt. Precambrian Research 55, 539–552.
Rushmer, T., 1991. Partial melting of two amphibolites: contrasting experimental results under fluid-absent conditions. Contributions to Mineralogy and Petrology 107, 41–59.
Safonov, O.G., Tatarinova, D.S., van Reenen, D.D., Golunova, M.A., Yapaskurt, V.O., 2014. Fluid-assisted interaction of peraluminous metapelites with trondhjemitic magma within the Petronella shear-zone, Limpopo Complex, South Africa. Precambrian Research 253, 114–145.
Santosh, M., Omori, S., 2008. CO_2 flushing: a plate tectonic perspective. Gondwana Research 13, 86–102.
Santosh, M., Wada, H., 1993. Microscale isotopic zonation in graphite crystals: evidence for channelled CO_2 influx in granulites. Earth and Planetary Science Letters 119, 19–26.
Santosh, M., Jackson, D.H., Harris, N.B.W., Mattey, D.P., 1991. Carbonic fluid inclusions in South Indian granulites: evidence for entrapment during charnockite formation. Contributions to Mineralogy and Petrology 108, 318–330.
Sarangi, S., Sarkar, A., Srinivasan, R., Patel, S.C., 2012. Carbon isotope studies of auriferous quartz carbonate veins from two orogenic gold deposits from the Neoarchean Chitradurga schist belt, Dharwar craton, India: evidence for mantle/magmatic source of auriferous fluid. Journal of Asian Earth Sciences 52, 1–11.
Satish-Kumar, M., 2005. Graphite-bearing CO_2-fluid inclusions in granulites: insights on graphite precipitation and carbon isotope evolution. Geochimica et Cosmochimica Acta 69, 3841–3856.
Satish-Kumar, M., Santosh, M., 1998. A petrological and fluid inclusion study of calc-silicate–charnockite associations from southern Kerala, India: implications for CO_2 influx. Geological Magazine 135, 27–45.
Satish-Kumar, M., Yurimoto, H., Itoh, S., Cesare, B., 2011. Carbon isotope anatomy of a single graphite crystal in a metapelitic migmatite revealed by high-spatial resolution SIMS analysis. Contributions to Mineralogy and Petrology 162, 821–834.
van Schalkwyk, J.F., van Reenen, D.D., 1992. High-temperature hydration of ultramafic granulites from the Southern Marginal Zone of the Limpopo Belt by infiltration of CO_2-rich fluid. Precambrian Research 55, 337–352.
Scheele, N., Hoefs, J., 1992. Carbon isotope fractionation between calcite, graphite and CO_2: an experimental study. Contributions to Mineralogy and Petrology 112, 35–45.
Schürmann, L.W., Ward, J.H.W., Horstmann, U.E., Jordaan, L.J., Eaton, B., 2000. Carbonate dykes associated with Archean lode-Au mineralisation, Barberton greenstone belt, South Africa. Journal of African Earth Sciences 30, 249–266.
Shengelia, D.M., Akhvlediani, R.A., Ketskhoveli, D.N., 1979. The graphite geothermometer. Doklady Akademii Nauk SSSR 235, 132–134.
Sisson, T.W., Ratajeski, K., Hankins, W.B., Glazner, A.F., 2005. Voluminous granitic magmas from common basaltic sources. Contributions to Mineralogy and Petrology 148, 635–661.
Skjerlie, K.P., Johnston, A.D., 1993. Fluid-absent melting behavior of an F-rich tonalitic gneiss at mid-crustal pressures: implications for the generation of anorogenic granites. Journal of Petrology 34, 785–815.
Skjerlie, K.P., Patino Douce, A., 1995. Anatexis of interlayered amphibolite and pelite at 10 kbar: effect of diffusion of major components on phase relations and melt fraction. Contributions to Mineralogy and Petrology 122, 62–78.
Smit, C.A., van Reenen, D.D., 1997. Deep crustal shear zone, high-grade tectonites, and associated metasomatic alteration in the Limpopo Belt, South Africa: implications for deep crustal processes. Journal of Geology 106, 37–57.
Smit, C.A., Roering, C., van Reenen, D.D., 1992. The structural framework of the Southern Marginal Zone of the Limpopo Belt, South Africa. Precambrian Research 55, 51–67.
Smit, C.A., Van Reenen, D.D., Gerya, T.V., Perchuk, L.L., 2001. P-T conditions of decompression of the Limpopo high-grade terrain: record from shear zones. Journal of Metamorphic Geology 19, 249–268.
Smit, C.A., van Reenen, D.D., Roering, C., Boshoff, R., Perchuk, L.L., 2011. Neoarchean to Paleoproterozoic evolution of the polymetamorphic Central Zone of the Limpopo Complex. Geological Society of America Memoirs 207, 213–244.
Smit, C.A., van Reenen, D.D., Roering, C., 2014. Role of fluids in the exhumation of the Southern Marginal Zone of the Limpopo Complex, South Africa. Precambrian Research 253, 81–95.
Steele-MacInnis, M., Bodnar, R.J., Naden, J., 2011. Numerical model to determine the composition of H_2O–NaCl–$CaCl_2$ fluid inclusions based on microthermometric and microanalytical data. Geochimica et Cosmochimica Acta 75, 21–40.
Sterner, S.M., Pitzer, K.S., 1994. An equation of state for carbon dioxide valid from zero to extreme pressures. Contributions to Mineralogy and Petrology 117, 362–374.
Stevens, G., 1991. Vapor-absent Melting in Metapelite During the 2700 Ma Limpopo Metamorphic Event in South Africa: Further Evidence of the Granite-Granulite Link. (Master Degree Dissertation). Rand Africaans University, Johannesburg.
Stevens, G., 1997. Melting, carbonic fluids and water recycling in the deep crust: an example from the Limpopo Belt, South Africa. Journal of Metamorphic Geology 15, 141–154.
Stevens, G., Clemens, J.D., 1993. Fluid-absent melting and the roles of fluids in the lithosphere: a slanted summary? Chemical Geology 108, 1–17.
Stevens, G., van Reenen, D.D., 1992. Partial melting and the origin of metapelitic granulites in the Southern Marginal Zone of the Limpopo Belt, South Africa. Precambrian Research 55, 303–319.
Taylor, J., Nicoli, G., Stevens, G., Frei, D., Moyen, J.-F., 2014. The process that control leucosome composition in metasedimentary granulites: perspectives from the Southern Marginal Zone. Limpopo Belt, South Africa. Journal of Metamorphic Geology 32, 713–742.
Todd, C.S., Evans, B.W., 1993. Limited fluid-rock interaction at marble-gneiss contacts during Cretaceous granulite-facies metamorphism, Seward Peninsula, Alaska. Contributions to Mineralogy and Petrology 114, 27–41.
Touret, J.L.R., 1971. Le faciès granulite en Norvège méridionale. II Les inclusions fluides. Lithos 4, 423–436.
Tracy, R.J., Robinson, P., 1988. Silicate-sulfide-oxide-fluid reactions in granulite-grade pelitic rocks, central Massachusetts. American Journal of Science 288, 45–74.
Tsunogae, T., Miyano, T., van Reenen, D.D., Smit, C.A., 2004. Ultrahigh-temperature metamorphism of the southern marginal zone of the Archean Limpopo Belt, South Africa. Journal of Mineralogical and Petrological Sciences 99, 213–224.
Tuinstra, F., Koenig, J.L., 1970. Raman spectrum of graphite. The Journal of Chemical Physics 53, 1126–1130.
Tuttle, O.F., Bowen, N.L., 1958. Origin of granite in the light of experimental studies in the system $NaAlSi_3O_8$–$KAlSi_3O_8$–SiO_2–H_2O. Geological Society of America Memoirs 74, 1–146.
Valley, J.W., 1986. Stable isotope geochemistry of metamorphic rocks. Reviews in Mineralogy. 16. Mineralogical Society of America, pp. 445–490.

Vennemann, T.W., Smith, H.S., 1992. Stable isotope profile across the orthoamphibole isograde in the Southern Marginal Zone of the Limpopo Belt, South Africa. Precambrian Research 55, 365–397.
Vielzeuf, D., Holloway, J.R., 1988. Experimental determination of the fluid-absent melting relations in the pelitic system. Consequences for crustal differentiation. Contributions to Mineralogy and Petrology 98, 257–276.
Wada, H., Tomita, T., Matsuura, K., Iuchi, K., Ito, M., Morikiyo, T., 1995. Graphitization of carbonaceous matter during metamorphism with references to carbonate and pelitic rocks of contact and regional metamorphism, Japan. Contributions to Mineralogy and Petrology 118, 217–228.
Watkins, J.M., Clemens, J.D., Treloar, P.J., 2007. Archaean TTGs as sources of younger granitic magmas: melting of sodic metatonalites at 0.6–1.2 GPa. Contributions to Mineralogy and Petrology 154, 91–110.
Watson, E.B., Brenan, J.M., 1987. Fluids in the lithosphere, 1. Experimentally determined wetting characteristics of CO_2-H_2O fluids, their implications for fluid transport, host-rock physical properties, and fluid inclusion formation. Earth and Planetary Science Letters 85, 497–515.
White, R.W., Powell, R., Holland, T.J.B., Johnson, T.E., Green, E.C.R., 2014. New mineral activity–composition relations for thermodynamic calculations in metapelitic systems. Journal of Metamorphic Geology 32, 261–286.
Whitney, D.L., 1992. Origin of CO_2-rich fluid inclusions in leucosomes from the Skagit migmatites, North Cascades, Washington, USA. Journal of Metamorphic Geology 10, 715–725.
Whitney, D.L., Evans, B.W., 2010. Abbreviations for names of rock-forming minerals. American Mineralogist 95, 185–187.
Wolf, M.B., Wyllie, P.J., 1994. Dehydration-melting of amphibolite at 10 kbar: the effects of temperature and time. Contributions to Mineralogy and Petrology 115, 369–383.
Zeck, H.P., 1970. An erupted migmatite from Cerro del Hoyazo, SE Spain. Contributions to Mineralogy and Petrology 26, 225–246.
Zeh, A., Jaguin, J., Poujol, M., Boulvais, P., Block, S., Paquette, J.-L., 2013. Juvenile crust formation in the northeastern Kaapvaal craton at 2.97 Ga – implication for Archean terrane accretion, and source of the Pietersburg gold. Precambrian Research 233, 20–43.
Zhang, C., Duan, Z., 2009. A model for C–O–H fluid in the Earth's mantle. Geochimica et Cosmochimica Acta 73, 2089–2102.
Zhang, C., Duan, Z., 2010. GFluid: an Excel spreadsheet for investigating C–O–H fluid composition under high temperatures and pressures. Computers & Geosciences 36, 569–572.
Zhu, C., Sverjensky, D.A., 1992. F-Cl-OH partitioning between biotite and apatite. Geochimica et Cosmochimica Acta 56, 3435–3467.